

MolVision: Molecular Property Prediction with Vision Language Models

Deepan Adak¹, Yogesh Singh Rawat², Shruti Vyas²
¹NIT Kurukshetra, ²University of Central Florida

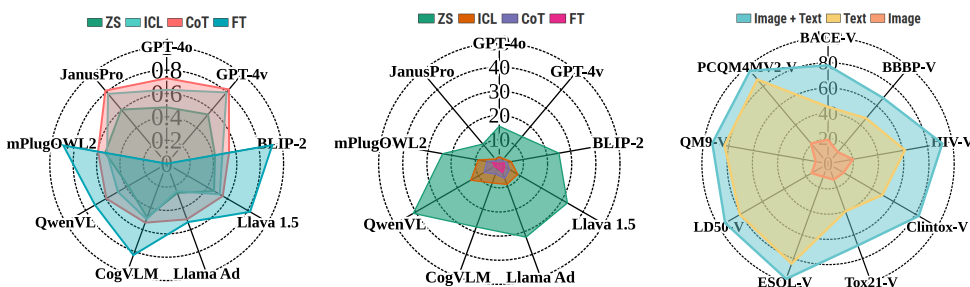


Figure 1: **MolVision overview**: Average performance comparison of models in zero-shot (ZS), in-context (ICL), chain-of-thoughts (CoT), and finetuning (FT) for classification (*Left* ↑) and regression tasks (*Center* ↓). (*Right*): Impact of using visual information on model performance (↑) (JanusPro).

Abstract

Molecular property prediction is a fundamental task in computational chemistry with critical applications in drug discovery and materials science. While recent works have explored Large Language Models (LLMs) for this task, they primarily rely on textual molecular representations such as SMILES/SELFIES, which can be ambiguous and structurally less informative. In this work, we introduce MolVision, a novel approach that leverages Vision-Language Models (VLMs) by integrating both molecular structure as images and textual descriptions to enhance property prediction. We construct a benchmark spanning ten diverse datasets, covering classification, regression and description tasks. Evaluating nine different VLMs in zero-shot, few-shot, and fine-tuned settings, we find that visual information improves prediction performance, particularly when combined with efficient fine-tuning strategies such as LoRA. Our results reveal that while visual information alone is insufficient, multimodal fusion significantly enhances generalization across molecular properties. Adaptation of vision encoder for molecular images in conjunction with LoRA further improves the performance. The code and data is available at : <https://molvision.github.io/MolVision/>.

1 Introduction

Recent advancements in Large Language Models (LLMs) have revolutionized natural language understanding and generation across multiple domains [1]. Models such as GPT [2, 3], LLaMA [4], and Mistral [5] have demonstrated exceptional capabilities in reasoning, knowledge retrieval, and complex problem-solving. Extending beyond pure text-based reasoning, Vision-Language Models (VLMs) integrate visual and textual modalities [1, 6, 7, 8], enabling them to perform tasks such as image captioning, visual question answering, and multimodal retrieval with remarkable success. While VLMs have been extensively explored in computer vision and NLP applications, their potential in scientific domains—particularly in chemistry—remains largely unexplored. Given that molecular

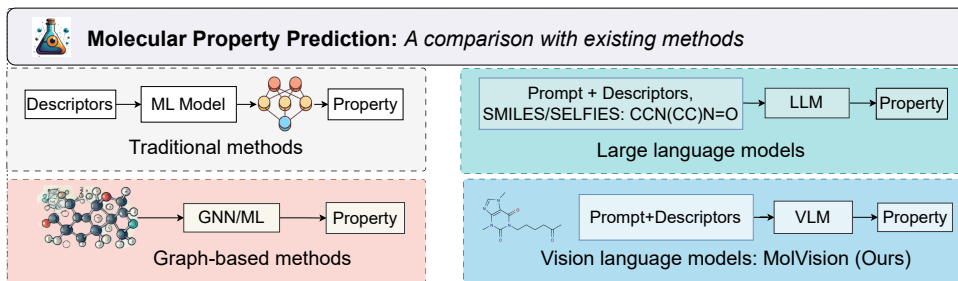


Figure 2: **MolVision comparison:** Comparison of relevant molecular property prediction approaches.

structures are inherently visual, leveraging vision in molecular analysis presents an exciting, yet underexplored, research direction.

Recent works such as ChemLLM [9] and ChemLLM-Bench [10] have begun to explore LLMs for molecular property prediction. These methods primarily rely on textual molecular representations, such as SMILES and SELFIES, which have been widely used in cheminformatics for decades. However, these representations have notable limitations, including their non-uniqueness and syntactic instability, where structurally identical molecules may have vastly different textual encodings. This ambiguity introduces challenges for LLMs, which process molecular structures as linear strings, potentially overlooking key structural relationships. While some approaches attempt to improve these representations through graph-based models [11], the integration of easily available visual molecular data remains largely unexplored in this domain.

Incorporating visual information has the potential to significantly enhance molecular property prediction. Chemists usually analyze molecular structures using bond-line or skeletal diagrams to infer properties such as reactivity, toxicity, and solubility. These visual representations inherently encode structural and spatial information that textual descriptors may fail to capture. For example, subtle differences in geometry, stereochemistry, or electron delocalization can have profound effects on molecular properties, yet are difficult to represent accurately in SMILES format alone. By leveraging VLMs, which are designed to process both visual and textual inputs, we aim to bridge this gap and improve predictive modeling in cheminformatics.

To this end, we introduce MolVision, a multimodal benchmark for molecular property prediction. In contrast to prior works MolVision integrates both textual and visual representations (Figure 2). Our benchmark spans ten diverse datasets, covering classification, regression and description tasks across a wide range of molecular properties, including toxicity, solubility, and bioactivity. We evaluate nine different VLMs in zero-shot, few-shot, and fine-tuned settings, providing a comprehensive analysis of their performance in this domain (Figure 1). We also propose a simple contrastive strategy to adapt visual component of VLMs for this domain and demonstrate its effectiveness for property prediction.

Through extensive experimentation, we uncover several key insights. First, while VLMs struggle in zero-shot settings, their performance improves significantly with in-context learning and fine-tuning. Second, efficient adaptation techniques such as LoRA enhance the predictive accuracy and generalization to unseen molecular properties. Third, while visual information alone is insufficient for accurate property prediction, combining molecular images with textual representations yields notable performance gains specifically for larger molecules. These findings suggest that vision-augmented molecular modeling presents a promising avenue for future research in AI-driven chemistry, with numerous potential applications. We make the following contributions:

- We introduce MolVision, a novel approach for molecular property prediction, integrating molecular structure images with textual representations.
- We present a multimodal benchmark and systematically assess nine state-of-the-art VLMs in zero-shot, few-shot, and fine-tuned settings across ten datasets highlighting their strengths and limitations for property prediction.
- We show that efficient adaptation of VLMs for property prediction enhances both performance and generalization, and that combining visual and textual data significantly improves molecular property prediction.
- We propose a simple contrastive strategy, implemented with LoRA, to efficiently adapt vision aspect of VLMs for this domain and demonstrate its effectiveness for property prediction.

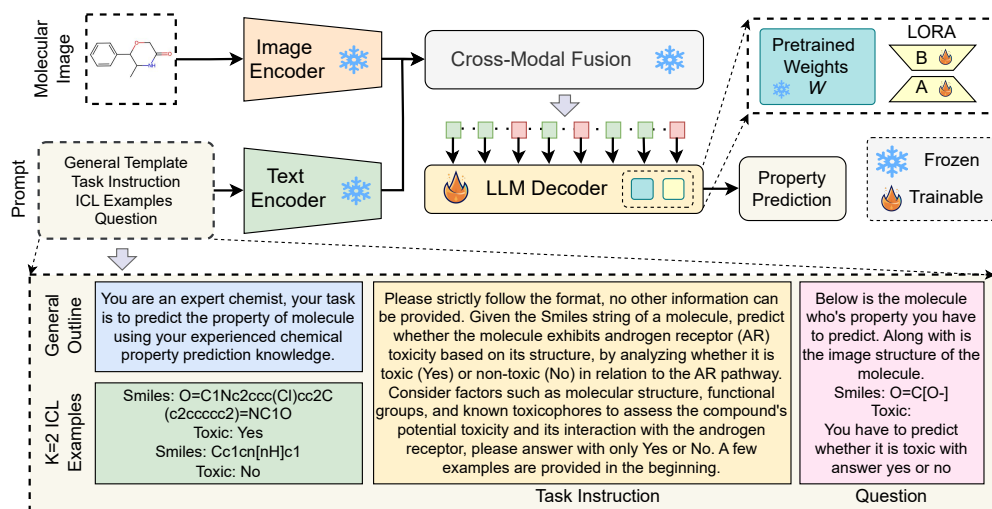


Figure 3: **Overview of visual-textual approach for property prediction:** The image representation along with textual description are used as input by the VLM where the image is encoded by a vision encoder and textual description is encoded by a text encoder. These multimodal features are used to generate the output with the help of a decoder. We show template prompt used for property prediction, including general outline, task instruction, in-context learning (ICL with $k=2$), and an image prompt.

2 Related works

Property prediction: Prior research in molecular property prediction has explored various methods and representations [12]. Traditional approaches, like molecular fingerprints [13, 14] and descriptors [15], rely on expert knowledge but are limited in capturing complex data relationships. Recently, machine learning techniques [16, 17, 18], particularly graph-based methods like graph convolutional networks (GCNs) [19], have gained prominence for capturing molecular interactions. Additionally, deep learning models, including RNNs, CNNs, and transformers [20, 21, 22, 23, 24], have shown strong performance in modeling structural and sequential information from molecular data.

Multimodal foundational models: Recent advances in Foundational Models [5, 4, 25] have shown the ability of multimodal LLMs to process both vision and language. These models integrate vision encoders [26, 27] with LLMs [28, 4] for generating text responses. Models like Llama Adapter V2 [7] and Flamingo [29] explored multimodal structures. Typically, these models pre-train on image caption datasets [30, 31] and fine-tune on task-specific datasets [32]. Models such as Llava 1.5 [33] and QwenVL [34] are designed for instruction-following tasks but may struggle with science-specific challenges like computational chemistry.

Foundation models for property prediction: Recent efforts have explored LLMs for property prediction, such as ChemLLM [9], ChemLLMBench [10], and Nach0 [35]. ChemLLM [9] utilizes ChemData, an instruction-tuning dataset, to address the need for specialized models in chemistry. Guo et al. [10] assess LLMs in chemistry, focusing on understanding and reasoning tasks with zero-shot and few-shot learning. In [36], the authors propose to utilize graphical structure with LLMs for molecule captioning, IUPAC name prediction, and molecule-text retrieval. In contrast, our work examines the role of multimodal vision-language models, incorporating visual and textual data for molecular property prediction, a first-of-its-kind exploration.

3 Visual language models for property prediction

We propose use of visual information, in the form of molecular images, alongside textual descriptions to improve property prediction. Images provide structural insights that are challenging to interpret from text alone. A vision-language model processes both the image and text prompt to generate a textual output, as shown in Figure 3. The input image is divided into patches, which are converted into tokens for the vision encoder (e.g., ViT [37]). The textual prompt is passed through a text encoder (e.g., BERT [37]), and the visual and textual features are fused via multi-modal learning (e.g., using Q-Former). LLM decoder (e.g., a transformer model) uses these fused features for text generation.

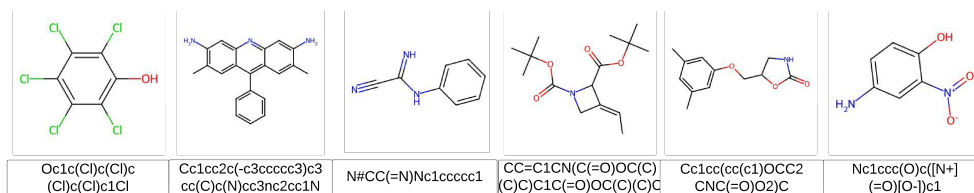


Figure 4: **Sample visual and textual representation pairs:** The images in top row shows skeletal structure of molecules and bottom row shows their corresponding SMILES representations.

Text prompt: The prompt consists of three components passed to the text encoder: 1) *General outline* provides an overview of the task, 2) *Task instruction* includes detailed task-specific guidance, and 3) *Question* requests the model’s answer in a specific format. For in-context learning and chain-of-thoughts, additional information like examples or reasoning steps is included (Figure 3).

3.1 Model variants

We study three different setups: 1) zero-shot, 2) few-shot, and 3) fine-tuning on training data.

Zero-shot: The model is evaluated without fine-tuning or in-context examples.

Few-shot: We use two approaches: 1) *In-context Learning (ICL)*: traditional prompting (labeled ICL) and *Chain of Thought (CoT) Prompting*. Traditional ICL constructs prompts with examples similar to the input, enabling the model to learn relationships in the new domain. CoT prompting enhances reasoning by guiding the model through intermediate steps. In cheminformatics, molecular similarity is often quantified using methods like similarity and distance metrics. For selecting few-shot samples, we use the Tanimoto index, an effective parameter for similarity prediction [34].

Finetuning: Vision-language models (VLMs) possess a substantial number of trainable parameters, rendering traditional fine-tuning impractical as all model parameters undergo gradient updates simultaneously. In our study, we adopt LoRA (Low-Rank Adaptation) [38] for efficient fine-tuning, a technique that significantly reduce the number of trainable parameters. LoRA achieves this by updating weights through a pair of trainable rank decomposition matrices, which operate in parallel with existing weight matrices, while keeping the original pre-trained weights frozen during fine-tuning. We only adapt the LLM decoder keeping other components frozen during this finetuning to preserve the generalization capabilities of vision and text encoders (Figure 3).

3.2 Model architectures

We study nine different state-of-the-art visual language models in this study. This includes both closed-source and open-source models. In open-source, we experimented with Janus-Pro 7B [39], BLIP-2 [37], Llava 1.5 [33], Llama Adapter V2 [7], CogVLM [40], Qwen-VL [34], and mPLUGOWL2 [41]. For closed-source, we experimented with GPT-4V and GPT-4o [1].

4 MolVision benchmark

In this section, we introduce the MolVision benchmark, which includes ten diverse datasets. These datasets cover a wide range of properties, such as molecular weight, topological polar surface area, and toxicity, and encompass classification, regression and description tasks. A summary in Table 1.

Tasks: VLMs generate textual outputs based on image and text prompts. For classification, we frame the task as a True/False question, where the model predicts whether a molecule inhibits a target property. For regression, the model generates a numerical value representing the target property and for description task, the model generates textual output.

Dataset curation: We incorporate both molecular skeletal structures as images and SMILES/SELFIES representations. Existing property prediction datasets primarily focus on textual representations like SMILES, lacking structural images. To address this, we augment these datasets with skeletal images generated using RDKit [42]. Figure 4 illustrates examples of skeletal (bond-line) structures alongside their SMILES representations. RDKit also enables conversion between SMILES and SELFIES, allowing us to explore diverse molecular encodings and enhance model robustness.

4.1 Benchmark datasets

The curation process provides both image representations corresponding to each molecule along with a formatted prompt which is derived through manual engineering. The benchmark consists of the following datasets (more details in Appendix): **BACE-V** is derived from BACE (Binary Activity of Chemical Entities) dataset [43] which is widely used for binary classification in bioactivity prediction, particularly for BACE-1 inhibitors linked to Alzheimer’s. **BBBP-V** is based on the Blood-Brain Barrier Penetration (BBBP) dataset [44], which provides binary labels for BBB penetration. **HIV-V** is based on the HIV [45] where we focus on predicting HIV replication inhibition. **Clintox-V** is derived from ClinTox dataset [43] and our focus is on predictions of clinical toxicity and FDA approval status. **Tox21-V** is based on the Tox21 dataset [46] and focuses on predicting chemical toxicity, critical for environmental safety. **ESOL-V** is based on the ESOL dataset [47], and focus on predicting aqueous solubility of organic compounds. **LD50-V** is based on the LD50 [48] and focuses on acute toxicity. **QM9-V** is derived from the QM9 [49] and focuses on quantum chemical properties. **PCQM4Mv2-V** is derived from the PCQM4Mv2 dataset [50] and focuses on predicting the HOMO-LUMO gap. **ChEBI20-V** is derived from the Chemical Entities of Biological Interest (ChEBI) [51] database and focuses on generating accurate textual descriptions of molecular structures.

Table 1: *MolVision benchmark details:* Statistics of datasets used in this study.

Dataset	Train	Test	Property
Classification			
BACE-V	1,210	303	Bioactivity
BBBP-V	1,640	410	BBB Pen.
HIV-V	32,902	8,225	HIV activity
ClinTox-V	1,193	298	Toxicity
Tox21-V	6,265	1,566	Toxicity
Regression			
ESOL-V	902	226	Solubility
LD50-V	5,908	1,477	Toxicity
QM9-V	107K	27K	Quantum
PCQM4Mv2-V	3.0M	0.7M	Quantum
Molecular Description			
ChEBI-V	32,000	8,000	Description

5 Experiments and results

Next, we provide evaluations on MolVision benchmark followed by some discussion and analysis.

Evaluation metrics: We evaluate classification performance using Accuracy and F1 Score. We evaluate classification using Accuracy and F1 Score, where Accuracy measures correct predictions, and F1 Score balances precision and recall. For regression, we use mean absolute error (MAE) and root mean square error (RMSE) to quantify prediction deviations. Molecular description tasks are assessed with BLEU-2, BLEU-4, ROUGE-1, ROUGE-2, ROUGE-L, and METEOR, capturing n-gram precision, sequence overlap, and semantic similarity.

5.1 Benchmarking results

All experiments are conducted with a temperature of 0 (unless stated) to reduce prediction volatility.

Zero-shot: VLMs are trained on large-scale datasets to learn associations between visual and textual features. However, property prediction presents a distinct challenge, differing from their training domain. Figures 1 (left and center) show zero-shot results across all datasets, where performance remains low for most models, except for proprietary models GPT-4o and GPT-4v. (More in Appendix.)

Few-shot: Tables 2 and 3 present few-shot ICL performance for classification and regression tasks, respectively. All models show performance gains over zero-shot, though Llama Adapter v2 7B and Qwen VL consistently underperform with classification accuracy below 48% and high regression errors. BBBP-V and QM9 remain challenging datasets, while Tox21-V and LD50 yield comparatively better results. As expected, closed models such as GPT-4o and GPT-4v achieved the best performance across most datasets however Janus-Pro 7B performed better on certain datasets. The performance was followed by Llava 1.5 13B and BLIP-2 as the second best open-source models for classification and regression, respectively. Table 3 also reports CoT prompting results for regression, showing further improvements, also seen in classification tasks (Figure 1, more info in Appendix).

Finetuning: Table 4 presents classification results after model adaptation, showing significant performance improvements with fine-tuning. A similar trend is observed for regression tasks, where adaptation reduces prediction error (Figure 1). Detailed results are provided in the Appendix. Overall, BLIP-2 achieves the best performance across both classification and regression tasks, while mPlugOWL2 remains competitive in classification but underperforms in regression. Table 5 show

Table 2: *Few-shot performance for classification tasks*: A comparison of accuracy (f1-score) on property prediction task using in-context learning (ICL with k=2). († - fully supervised training)

Models	BACE-V ↑	BBBP-V ↑	HIV-V ↑	ClinTox-V ↑	Tox21-V ↑	Average ↑
GNN Models						
UniMol [11] †	0.78(0.67)	0.82(0.70)	0.82(0.73)	0.94(0.83)	0.77(0.65)	0.83(0.72)
Molca [36] †	0.79(0.73)	0.74(0.72)	0.89(0.84)	0.93(0.84)	0.80(0.72)	0.83(0.77)
LLM [ICL k=2]						
Guo et. al. [52]	0.49(0.40)	0.46(0.46)	0.86(0.80)	0.57(0.36)	0.57(0.52)	0.59(0.51)
Davinci-003	0.65(0.64)	0.39(0.37)	0.78(0.83)	0.84(0.85)	0.68(0.51)	0.67(0.64)
ChemLLM[9]	0.18(0.12)	0.12(0.08)	0.19(0.09)	0.21(0.13)	0.18(0.09)	0.18(0.10)
Gal-1.3B [53]	0.38(0.29)	0.42(0.26)	0.33(0.23)	0.40(0.34)	0.49(0.32)	0.40(0.29)
Gal-6.7B [53]	0.41(0.30)	0.44(0.28)	0.35(0.25)	0.43(0.36)	0.52(0.34)	0.44(0.31)
VLM [ICL k=2]						
GPT-4o	0.56(0.53)	0.77(0.81)	0.82(0.56)	0.59(0.44)	0.42(0.58)	0.63(0.58)
GPT-4v	0.72(0.66)	0.63(0.60)	0.95(0.44)	0.96(0.94)	0.72(0.52)	0.80(0.63)
Janus Pro 7B	0.78(0.71)	0.68(0.62)	0.92(0.52)	0.83(0.56)	0.69(0.49)	0.78(0.58)
BLIP-2	0.36(0.52)	0.37(0.29)	0.60(0.30)	0.34(0.36)	0.75(0.42)	0.48(0.38)
Llava 1.5 13B	0.49(0.48)	0.44(0.39)	0.24(0.34)	0.64(0.76)	0.81(0.31)	0.52(0.46)
Llama Ad v2 7B	0.28(0.29)	0.18(0.11)	0.19(0.17)	0.29(0.12)	0.31(0.21)	0.25(0.18)
CogVLM	0.48(0.51)	0.40(0.37)	0.31(0.21)	0.64(0.62)	0.69(0.65)	0.50(0.47)
QwenVL	0.69(0.46)	0.30(0.12)	0.28(0.36)	0.52(0.48)	0.62(0.63)	0.48(0.41)
mPlugowl2	0.59(0.32)	0.35(0.38)	0.62(0.29)	0.34(0.42)	0.69(0.56)	0.52(0.39)

Table 3: *Few-shot performance for regression*: A comparison of error in prediction using in-context learning (ICL k=2) and chain-of-thoughts (CoT) with traditional and LLM based approaches.

Model	ESOL-V ↓		LD50-V ↓		QM9-V ↓		PCQM4M-V ↓		Average ↓	
Traditional approaches										
GenRA[54]	-		0.58		-		-		-	
Unimol [11]	0.788		-		0.00467		0.070		-	
Large Language Models										
GPT-3.5	4.24		11.67		13.52		1.81		5.81	
Llama2 13B	27.71		49.22		78.92		102.92		64.69	
Mistral 13B	33.21		27.46		66.80		88.90		54.09	
ChemLLM [9]	23.42		33.91		147.10		29.01		58.36	
GAL-1.3B [53]	18.92		40.49		140.92		29.92		-	
Gal-6.7B [53]	13.47		38.02		128.90		28.48		-	
Molca [36]	1.849		0.982		4.889		0.802		-	
Vision-Language Models										
	ICL	CoT								
GPT-4o	0.98	0.77	0.87	0.60	8.38	5.24	0.68	0.53	2.73	1.78
GPT-4v	0.99	0.71	0.71	0.59	8.62	4.66	0.77	0.66	2.78	1.66
Janus-Pro 7B	0.61	0.89	0.72	0.60	8.53	4.42	0.62	0.38	2.52	1.57
BLIP-2	1.99	1.07	0.73	0.49	16.01	10.09	1.30	1.25	5.01	3.23
Llava 1.5 13B	6.01	2.18	0.94	0.69	27.00	15.21	1.42	1.49	8.84	4.89
Llama Ad v2 7B	3.08	2.17	3.36	2.12	28.09	19.24	4.06	2.36	9.15	6.47
CogVLM	1.26	1.21	3.47	0.78	25.85	15.15	1.44	1.24	8.50	4.59
Qwen VL	3.96	2.89	1.06	0.63	38.92	18.08	10.61	9.56	13.64	7.29
mPlugOWL2	1.46	1.50	0.94	0.71	29.33	19.17	1.84	1.62	8.89	5.25

performance on molecular description task after finetuning. We observe that CogVLM outperforms other VLMs across all metrics and performs better than recent graph-based LLM.

Zero-shot generalization: Figure 5 shows results with zero-shot generalization where we adapted the model on one dataset and evaluated on others. As shown, the performance is better than few-shot (Table 2), however the performance is not as good as LoRA where the model was finetuned on the target dataset (Table 4). From Figure 5 we observe that after training on HIV-V dataset we get the best zero-shot average accuracy (61%) and best zero-shot avg F1-score is observed after training on BBBP-V. ClinTox-V and BBBP-V are the most difficult datasets for zero shot generalization with an average accuracy of 39% and 40%, respectively.

Table 4: **Classification performance after finetuning:** Accuracy (F1 score) comparison of models finetuned using LoRA. The best performing models are highlighted with bold text.

Models	BACE-V \uparrow	BBBP-V \uparrow	HIV-V \uparrow	ClinTox-V \uparrow	Tox21-V \uparrow	Average \uparrow
RF	0.79(0.76)	0.82(0.88)	0.87(0.52)	0.85(0.46)	0.83(0.26)	0.83(0.57)
XGBoost	0.81(0.77)	0.85(0.90)	0.87(0.55)	0.88(0.62)	0.84(0.33)	0.85(0.63)
ChemLLM [9]	0.18(0.12)	0.12(0.08)	0.19(0.09)	0.21(0.13)	0.18(0.09)	0.17(0.10)
Molca [36]	0.79(0.73)	0.74(0.72)	0.89(0.84)	0.93(0.84)	0.80(0.72)	0.83(0.77)
BLIP-2	0.86(0.83)	0.93(0.96)	0.92(0.76)	0.89(0.93)	0.99(0.80)	0.92(0.86)
Llava 1.5 13B	0.84(0.83)	0.86(0.88)	0.80(0.81)	0.70(0.72)	0.92(0.93)	0.82(0.83)
Llama Adapter v2 7B	0.52(0.48)	0.45(0.46)	0.43(0.42)	0.58(0.62)	0.68(0.69)	0.53(0.53)
CogVLM	0.72(0.71)	0.78(0.82)	0.85(0.83)	0.88(0.90)	0.93(0.93)	0.83(0.84)
Qwen VL	0.78(0.78)	0.70(0.72)	0.60(0.61)	0.71(0.64)	0.75(0.64)	0.71(0.68)
mPlugOWL2	0.86(0.82)	0.90(0.88)	0.90(0.91)	0.89(0.92)	0.94(0.96)	0.89(0.89)

Table 5: **Molecular description performance after finetuning:** Comparison of models finetuned using LoRA on the ChEBI dataset. The best performing models are highlighted with bold text.

Models	BLEU-2 \uparrow	BLEU-4 \uparrow	ROUGE-1 \uparrow	ROUGE-2 \uparrow	ROUGE-L \uparrow	METEOR \uparrow	Average \uparrow
MolT5 [55]	59.40	50.80	65.40	51.00	59.40	61.40	57.90
Molca [36]	62.00	53.10	68.10	53.70	61.80	65.10	60.60
BLIP-2	59.06	58.03	58.93	58.47	58.89	58.19	58.60
CogVLM	63.00	60.01	62.39	61.16	62.00	60.60	61.52
mPlugOWL2	51.93	49.64	51.56	50.67	51.33	50.06	50.87
Llava 1.5 13B	60.88	58.99	60.62	59.80	60.42	59.40	60.02
Llama Adapter v2 7B	46.60	44.65	46.27	45.50	46.07	45.00	45.68
Qwen VL	52.00	50.04	51.63	50.78	51.40	50.44	51.05

Table 6: **Impact of visual information:** A performance comparison showing the impact of visual information (molecular image) when used with textual description (SMILES). Accuracy is shown for classification (BACE-V, BBBP-V, HIV-V, Clintox-V (CV), Tox21-V (TV)), and MAE (LD50-V, QM9-V and PCQM4Mv2-V (PV)) and RMSE (ESOL-V) is shown for regression tasks.

Model	Input	BACE-V \uparrow	BBBP-V \uparrow	HIV-V \uparrow	CV \uparrow	TV \uparrow	ESOL-V \downarrow	LD50-V \downarrow	QM9-V \downarrow	PV \downarrow
BLIP-2	Text Only	0.71	0.76	0.69	0.64	0.78	9.89	7.80	31.76	11.31
	Image Only	0.15	0.09	0.10	0.13	0.18	32.16	31.23	149.12	36.96
	Image+Text	0.86	0.93	0.92	0.89	0.99	1.07	0.49	4.92	1.99
JanusPro	Text Only	0.45	0.47	0.62	0.50	0.40	1.23	1.16	20.94	2.09
	Image Only	0.19	0.12	0.20	0.14	0.13	21.57	12.49	125.03	16.20
	Image+Text	0.78	0.68	0.92	0.83	0.69	0.61	0.72	8.53	0.62

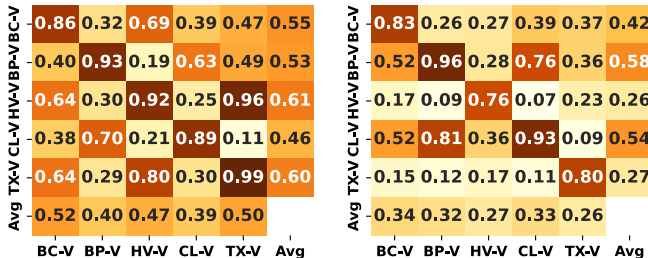


Figure 5: **Zero-shot generalization:** Visualization of accuracy (left) and F1-score (right) for zero-shot cross-dataset performance using BLIP-2. Each heatmap illustrates results from fine-tuning on one dataset (y-axis) and evaluating on others.

Models	Zero	ICL	CoT	LoRA
GPT-4v	2/1/2	1/3/1	1/1/2	-
GPT-4o	5/3/1	3/2/2	3/2/1	-
JanusPro 7B	1/2/3	2/1/3	2/3/3	-
BLIP-2	7/5/8	7/4/6	7/3/7	1/1/3
Llava1.5 13B	4/8/4	4/6/7	6/6/4	4/4/2
Llama v2 7B	9/7/9	9/8/9	9/8/9	6/6/6
CogVLM	4/6/5	6/5/4	8/5/5	3/2/1
Qwen VL	8/9/7	8/9/5	5/9/6	5/3/4
mPlugOWL2	3/4/6	5/7/8	4/7/8	2/5/5

Table 7: **Overall ranking:** Performance in terms of average ranking across datasets (classification/regression/description).

5.2 Comparison with existing methods

We compare our approach with traditional methods such as XGBoost, RF, GenRA [54], and Unimol [11], as well as recent LLM-based property prediction models that rely solely on text (ChemLLM-Bench [52] and ChemLLM [9]). Table 2 shows that incorporating visual information leads to better performance than LLMs using text alone. Table 3 compares VLMs with traditional models, where Janus-Pro, GPT-4o, and GPT-4v achieve competitive results on ESOL and LD50, though performance on QM9 and PCQM4M remains lower due to extensive training of traditional models on these

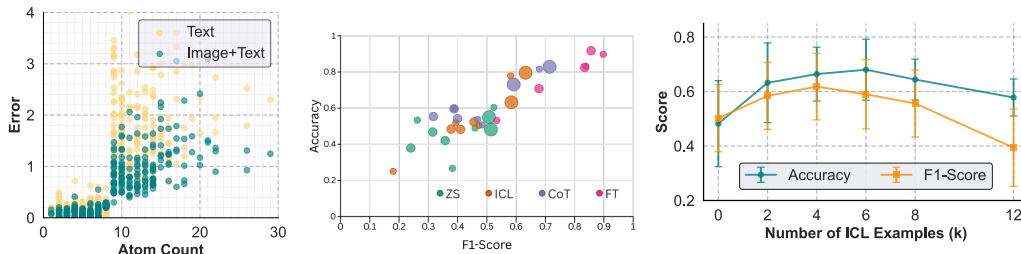


Figure 6: **Analysis on molecular-size, model-size and effect of in-context examples:** The first plot shows the impact of molecular size on regression error in LD50 with JanusPro, highlighting how visual data improves performance. The middle figure shows comparison of VLMs across datasets Accuracy vs F1 Score for zero shot (ZS), in-context (ICL), CoT and finetuning (FT). The bubble size represents the model’s parameter scale. The right figure shows variation in accuracy and f1-scores in case of different ICL examples for GPT-4o model.

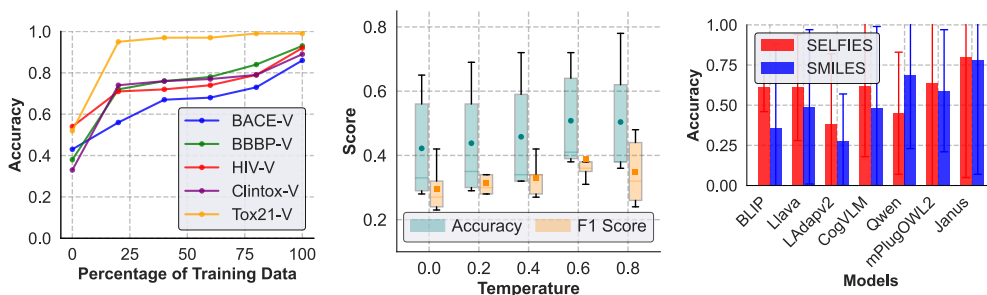


Figure 7: **Analysis on finetuning, temperature and SELFIES vs. SMILES:** The first plot shows the impact of percentage of finetuning data. The middle figure shows performance variation with temperature across datasets for BLIP2. The last figure shows analysis of SMILE vs SELFIES string for ICL k=2 across various models.

datasets. In classification tasks (Table 4), VLMs consistently outperform traditional approaches, with the largest gains on challenging datasets like BBBP-V. We also compare with a recent graph-based domain specific LLM approach Molca [36], and observe that our vision based approach provides better or comparable performance across all tasks and datasets (Table 3 and 5).

5.3 Discussion and analysis

This section provides further discussion and analysis for more insights into the benchmark.

Impact of visual data: Previously, we showed that VLMs outperform LLMs (Tables 2 and 3). Here, in Table 6, we analyze the impact of visual information within the same model by evaluating BLIP-2 and JanusPro in three configurations: (1) Image+Text (molecular structure images + SMILES), (2) Text Only (SMILES), and (3) Image Only (molecular images). We see that image-only inputs are insufficient, but augmenting text with visual data improves performance, showing the benefits of multimodal learning. Limitations and ethical considerations are discussed in Appendix.

Molecular size: We analyze the impact of molecular size on performance and find that larger molecules are more challenging, suggesting that longer representations are harder for models to interpret (Figure 6 (a)). We also observe that incorporating visual representations improves performance on larger molecules, further reinforcing the value of structural images in property prediction.

Capability of different models: After fine-tuning (Table 4), BLIP-2 achieves the highest accuracy across classification tasks, except for ClinTox-V, where mPlugOWL2 performs comparably. mPlugOWL2 ranks second overall, followed by CogVLM and Llava 1.5 13B, as confirmed in Table 7. BLIP-2 also excels in regression tasks.

Impact of model size on performance: Since VLMs are trained on large-scale datasets, their size generally correlates with performance. In our analysis of property prediction, we observe a similar trend, where larger models consistently outperform their smaller counterparts (Figure 6 (c)). Notably, while larger models perform better post-ICL, smaller models surpass them after fine-tuning.

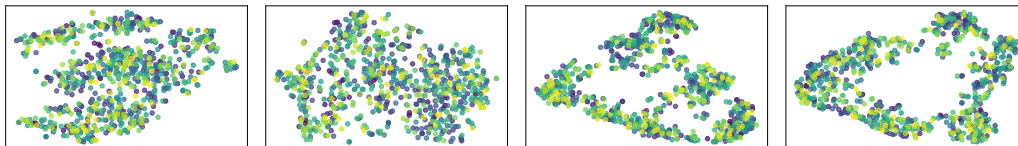


Figure 8: **Analyzing visual features:** The left two plots show t-SNE visualizations of visual encodings of BLIP-2 before and after cross-modal fusion respectively. The right two plots show corresponding t-SNE plots with the proposed contrastive loss using Tanimoto augmentation (T-Aug).

Table 8: **Performance comparison for proposed contrastive learning:** Evaluation of different contrastive learning approaches across multiple molecular datasets.

Method	BACE-V Acc(F1)	BBBP-V Acc(F1)	HIV-V Acc(F1)	Clintox-V Acc(F1)	Tox21-V Acc(F1)	ESOL-V (RMSE)	LD50-V (MAE)	QM9-V (MAE)	PCQM-V	Chebi-V (Average)
LoRA	0.86(0.83)	0.93(0.96)	0.92(0.76)	0.89(0.93)	0.99(0.80)	1.76	0.78	4.92	0.24	58.59
Aug	0.87(0.85)	0.94(0.95)	0.93(0.78)	0.90(0.94)	0.97(0.83)	0.90	0.20	4.09	0.21	60.98
T-Aug	0.91(0.88)	0.95(0.96)	0.95(0.84)	0.93(0.93)	0.98(0.89)	0.58	0.10	2.95	0.12	63.73

Effect of number of ICL examples: Figure 6 (a) shows that performance improves with more in-context examples but degrades beyond a certain point. This can be accredited to VLMs’ limitations in processing long prompts with excessive tokens.

Effect of amount of finetuning data: Figure 7 (left) show the impact of increasing finetuning data from 0% to 100% in 20% increments. We observe best performance with 100% data in all datasets, resulting in $\sim 40\%$ increase in performance.

Effect of temperature: Figure 7 shows how accuracy (F1-score) averaged across datasets vary with change in temperature. With most of the models (in supplementary) usually highest accuracy and F1-score is observed at lower temperatures (0.0-0.4) (in appendix), however, BLIP-2 showed better performance at higher temperatures (0.8).

SELFIES vs SMILES. SELFIES are more robust molecular representations, adhering to valence and ring constraints, thus avoiding invalid molecule generation [56]. In Figure 7 (right) we observe that with few exceptions, SELFIES provides better scores on most datasets.

5.4 Adaptation of vision encoder to molecular structures

To enhance the visual representation capability of VLMs in the molecular domain, we analyzed the vision embeddings of BLIP-2 using t-SNE and found them to be poorly clustered and non-discriminative—likely due to pretraining on natural images (Fig. 8). To address this, we fine-tuned the vision encoder using a contrastive learning objective (NT-Xent loss [57]) along with LoRA finetuning. We follow two strategies for identifying the positive pairs and use them in separate approaches. First approach uses augmented views of the same molecule (Aug, Table 8), and second approach uses structurally similar molecules identified via Tanimoto similarity (>0.85) (T-Aug). As shown in Fig. 8, the similarity-based approach leads to more distinct and meaningful clusters in the embedding space, capturing pharmacophoric patterns more effectively. This method significantly improves performance—reducing ESOL RMSE by 35%, LD50 MAE by 51%, and boosting classification accuracy and F1 scores by 2–4% over the base model. These results underscore the importance of domain-aware vision adaptation, and demonstrate that Tanimoto-guided contrastive learning offers a simple yet powerful enhancement for VLMs in molecular property prediction.

6 Conclusion

We present MolVision, a multimodal approach for molecular property prediction using vision-language models. We analyze zero-shot, few-shot, and fine-tuned models, combining 2D molecular structure images with textual representations. We provide evaluations on a wide variety of datasets covering classification, regression and description tasks, and demonstrate the benefits of visual information for molecular property prediction. Adaptation of vision encoder of VLMs to molecular data makes them more promising. This study will serve as a benchmark for further research exploring the use of easily available 2D visual information in multimodal molecular modeling.

7 Acknowledgment

This research has benefitted from the Microsoft Accelerating Foundation Models Research (AFMR) grant program.

References

- [1] OpenAI, J. Achiam, and et. al., “Gpt-4 technical report,” 2024.
- [2] J. Achiam, S. Adler, S. Agarwal, L. Ahmad, I. Akkaya, F. L. Aleman, D. Almeida, J. Altenschmidt, S. Altman, S. Anadkat, *et al.*, “Gpt-4 technical report,” *arXiv preprint arXiv:2303.08774*, 2023.
- [3] L. Floridi and M. Chiriatti, “Gpt-3: Its nature, scope, limits, and consequences,” *Minds and Machines*, vol. 30, pp. 681–694, 2020.
- [4] H. Touvron, L. Martin, K. Stone, P. Albert, A. Almahairi, Y. Babaei, N. Bashlykov, S. Batra, P. Bhargava, S. Bhosale, D. Bikel, L. Blecher, C. C. Ferrer, M. Chen, G. Cucurull, D. Esiobu, J. Fernandes, J. Fu, W. Fu, B. Fuller, C. Gao, V. Goswami, N. Goyal, A. Hartshorn, S. Hosseini, R. Hou, H. Inan, M. Kardas, V. Kerkez, M. Khabsa, I. Kloumann, A. Korenev, P. S. Koura, M.-A. Lachaux, T. Lavril, J. Lee, D. Liskovich, Y. Lu, Y. Mao, X. Martinet, T. Mihaylov, P. Mishra, I. Molybog, Y. Nie, A. Poulton, J. Reizenstein, R. Rungta, K. Saladi, A. Schelten, R. Silva, E. M. Smith, R. Subramanian, X. E. Tan, B. Tang, R. Taylor, A. Williams, J. X. Kuan, P. Xu, Z. Yan, I. Zarov, Y. Zhang, A. Fan, M. Kambadur, S. Narang, A. Rodriguez, R. Stojnic, S. Edunov, and T. Scialom, “Llama 2: Open foundation and fine-tuned chat models,” 2023.
- [5] A. Q. Jiang, A. Sablayrolles, A. Mensch, C. Bamford, D. S. Chaplot, D. de las Casas, F. Bressand, G. Lengyel, G. Lample, L. Saulnier, L. R. Lavaud, M.-A. Lachaux, P. Stock, T. L. Scao, T. Lavril, T. Wang, T. Lacroix, and W. E. Sayed, “Mistral 7b,” 2023.
- [6] H. Liu, C. Li, Q. Wu, and Y. J. Lee, “Visual instruction tuning,” 2023.
- [7] P. Gao, J. Han, R. Zhang, Z. Lin, S. Geng, A. Zhou, W. Zhang, P. Lu, C. He, X. Yue, H. Li, and Y. Qiao, “Llama-adapter v2: Parameter-efficient visual instruction model,” 2023.
- [8] G. Team and et. al., “Gemini: A family of highly capable multimodal models,” 2024.
- [9] D. Zhang, W. Liu, Q. Tan, J. Chen, H. Yan, Y. Yan, J. Li, W. Huang, X. Yue, W. Ouyang, D. Zhou, S. Zhang, M. Su, H.-S. Zhong, and Y. Li, “Chemllm: A chemical large language model,” 2024.
- [10] T. Guo, K. Guo, B. Nan, Z. Liang, Z. Guo, N. V. Chawla, O. Wiest, and X. Zhang, “What can large language models do in chemistry? a comprehensive benchmark on eight tasks,” 2023.
- [11] S. Lu, Z. Gao, D. He, L. Zhang, and G. Ke, “Highly accurate quantum chemical property prediction with uni-mol+,” *arXiv preprint arXiv:2303.16982*, 2023.
- [12] C. Hasselgren and T. I. Oprea, “Artificial intelligence for drug discovery: Are we there yet?,” *Annual Review of Pharmacology and Toxicology*, vol. 64, p. 527–550, Jan. 2024.
- [13] R. N. Tazhigulov, J. Schiller, J. Oppenheim, and M. Winston, “Molecular fingerprints for robust and efficient ml-driven molecular generation,” 2022.
- [14] I. Kumar and P. K. Jha, “Coarse-grained configurational polymer fingerprints for property prediction using machine learning,” 2023.
- [15] R. Todeschini and V. Consonni, *Handbook of molecular descriptors*. John Wiley & Sons, 2008.
- [16] K. Choudhary and M. L. Kelley, “Chemnlp: A natural language-processing-based library for materials chemistry text data,” *The Journal of Physical Chemistry C*, vol. 127, p. 17545–17555, Aug. 2023.

- [17] H. Öztürk, A. Özgür, P. Schwaller, T. Laino, and E. Ozkirimli, “Exploring chemical space using natural language processing methodologies for drug discovery,” *Drug Discovery Today*, vol. 25, p. 689–705, Apr. 2020.
- [18] G. M. Hocky and A. D. White, “Natural language processing models that automate programming will transform chemistry research and teaching,” *Digital Discovery*, vol. 1, no. 2, p. 79–83, 2022.
- [19] J. Gilmer, S. S. Schoenholz, P. F. Riley, O. Vinyals, and G. E. Dahl, “Neural message passing for quantum chemistry,” in *International conference on machine learning*, pp. 1263–1272, PMLR, 2017.
- [20] Z. Wu, B. Ramsundar, E. N. Feinberg, J. Gomes, C. Geniesse, A. S. Pappu, K. Leswing, and V. Pande, “Moleculenet: a benchmark for molecular machine learning,” *Chemical science*, vol. 9, no. 2, pp. 513–530, 2018.
- [21] D. Weininger, “Smiles, a chemical language and information system. 1. introduction to methodology and encoding rules,” *Journal of Chemical Information and Computer Sciences*, vol. 28, no. 1, pp. 31–36, 1988.
- [22] B. Tang, S. T. Kramer, M. Fang, Y. Qiu, Z. Wu, and D. Xu, “A self-attention based message passing neural network for predicting molecular lipophilicity and aqueous solubility,” *Journal of cheminformatics*, vol. 12, pp. 1–9, 2020.
- [23] G. B. Goh, N. O. Hodas, and A. Vishnu, “Deep learning for computational chemistry,” *Journal of computational chemistry*, vol. 38, no. 16, pp. 1291–1307, 2017.
- [24] D. C. Elton, Z. Boukouvalas, M. D. Fuge, and P. W. Chung, “Deep learning for molecular design—a review of the state of the art,” *Molecular Systems Design & Engineering*, vol. 4, no. 4, pp. 828–849, 2019.
- [25] T. Brown, B. Mann, N. Ryder, M. Subbiah, J. D. Kaplan, P. Dhariwal, A. Neelakantan, P. Shyam, G. Sastry, A. Askell, *et al.*, “Language models are few-shot learners,” *Advances in neural information processing systems*, vol. 33, pp. 1877–1901, 2020.
- [26] Y. Fang, W. Wang, B. Xie, Q. Sun, L. Wu, X. Wang, T. Huang, X. Wang, and Y. Cao, “Eva: Exploring the limits of masked visual representation learning at scale,” 2022.
- [27] A. Radford, J. W. Kim, C. Hallacy, A. Ramesh, G. Goh, S. Agarwal, G. Sastry, A. Askell, P. Mishkin, J. Clark, G. Krueger, and I. Sutskever, “Learning transferable visual models from natural language supervision,” 2021.
- [28] L. Zheng, W.-L. Chiang, Y. Sheng, S. Zhuang, Z. Wu, Y. Zhuang, Z. Lin, Z. Li, D. Li, E. P. Xing, H. Zhang, J. E. Gonzalez, and I. Stoica, “Judging llm-as-a-judge with mt-bench and chatbot arena,” 2023.
- [29] J.-B. Alayrac, J. Donahue, P. Luc, A. Miech, I. Barr, Y. Hasson, K. Lenc, A. Mensch, K. Millican, M. Reynolds, R. Ring, E. Rutherford, S. Cabi, T. Han, Z. Gong, S. Samangooei, M. Monteiro, J. Menick, S. Borgeaud, A. Brock, A. Nematzadeh, S. Sharifzadeh, M. Binkowski, R. Barreira, O. Vinyals, A. Zisserman, and K. Simonyan, “Flamingo: a visual language model for few-shot learning,” 2022.
- [30] S. Changpinyo, P. Sharma, N. Ding, and R. Soricut, “Conceptual 12m: Pushing web-scale image-text pre-training to recognize long-tail visual concepts,” 2021.
- [31] T.-Y. Lin, M. Maire, S. Belongie, L. Bourdev, R. Girshick, J. Hays, P. Perona, D. Ramanan, C. L. Zitnick, and P. Dollár, “Microsoft coco: Common objects in context,” 2015.
- [32] A. Agrawal, J. Lu, S. Antol, M. Mitchell, C. L. Zitnick, D. Batra, and D. Parikh, “Vqa: Visual question answering,” 2016.
- [33] H. Liu, C. Li, Y. Li, and Y. J. Lee, “Improved baselines with visual instruction tuning,” 2024.
- [34] H. K. Bajusz D, Rác A, “Why is tanimoto index an appropriate choice for fingerprint-based similarity calculations?,” 2015.

- [35] M. Livne, Z. Miftahutdinov, E. Tutubalina, M. Kuznetsov, D. Polykovskiy, A. Brundyn, A. Jhunjhunwala, A. Costa, A. Aliper, A. Aspuru-Guzik, and A. Zhavoronkov, "nach0: Multimodal natural and chemical languages foundation model," 2024.
- [36] Z. Liu, S. Li, Y. Luo, H. Fei, Y. Cao, K. Kawaguchi, X. Wang, and T.-S. Chua, "Molca: Molecular graph-language modeling with cross-modal projector and uni-modal adapter," in *Proceedings of the 2023 Conference on Empirical Methods in Natural Language Processing*, pp. 15623–15638, 2023.
- [37] J. Li, D. Li, S. Savarese, and S. Hoi, "Blip-2: Bootstrapping language-image pre-training with frozen image encoders and large language models," 2023.
- [38] E. J. Hu, Y. Shen, P. Wallis, Z. Allen-Zhu, Y. Li, S. Wang, L. Wang, and W. Chen, "Lora: Low-rank adaptation of large language models," *arXiv preprint arXiv:2106.09685*, 2021.
- [39] X. Chen, Z. Wu, X. Liu, Z. Pan, W. Liu, Z. Xie, X. Yu, and C. Ruan, "Janus-pro: Unified multimodal understanding and generation with data and model scaling," *arXiv preprint arXiv:2501.17811*, 2025.
- [40] W. Wang, Q. Lv, W. Yu, W. Hong, J. Qi, Y. Wang, J. Ji, Z. Yang, L. Zhao, X. Song, J. Xu, B. Xu, J. Li, Y. Dong, M. Ding, and J. Tang, "Cogvlm: Visual expert for pretrained language models," 2024.
- [41] Q. Ye, H. Xu, G. Xu, J. Ye, M. Yan, Y. Zhou, J. Wang, A. Hu, P. Shi, Y. Shi, C. Li, Y. Xu, H. Chen, J. Tian, Q. Qian, J. Zhang, F. Huang, and J. Zhou, "mplug-owl: Modularization empowers large language models with multimodality," 2024.
- [42] G. Landrum, "Rdkit documentation," *Release*, vol. 1, no. 1-79, p. 4, 2013.
- [43] G. Subramanian, B. Ramsundar, V. Pande, and R. A. Denny, "Computational modeling of β -secretase 1 (bace-1) inhibitors using ligand based approaches," *Journal of Chemical Information and Modeling*, vol. 56, no. 10, pp. 1936–1949, 2016. PMID: 27689393.
- [44] O. T. Sakiyama H, Fukuda M, "Prediction of blood-brain barrier penetration (bbbp) based on molecular descriptors of the free-form and in-blood-form datasets. molecules.," 2021.
- [45] Y. SS, "The nci's aids antiviral drug screening program," 1995.
- [46] R. Huang, M. Xia, D.-T. Nguyen, T. Zhao, S. Sakamuru, J. Zhao, S. A. Shahane, A. Rossoshek, and A. Simeonov, "Tox21challenge to build predictive models of nuclear receptor and stress response pathways as mediated by exposure to environmental chemicals and drugs," *Frontiers in Environmental Science*, vol. 3, p. 85, 2016.
- [47] J. S. Delaney, "Esol: estimating aqueous solubility directly from molecular structure," *Journal of chemical information and computer sciences*, vol. 44, no. 3, pp. 1000–1005, 2004.
- [48] A. Karmaus, J. Fitzpatrick, D. Allen, G. Patlewicz, N. Kleinstreuer, and W. Casey, "Variability of ld50 values from rat oral acute toxicity studies: implications for alternative model development," *Society of Toxicology, San Antonio, TX*, vol. 3, pp. 11–15, 2018.
- [49] A. Jain, S. P. Ong, G. Hautier, W. Chen, W. D. Richards, S. Dacek, S. Cholia, D. Gunter, D. Skinner, G. Ceder, *et al.*, "Commentary: The materials project: A materials genome approach to accelerating materials innovation," *APL materials*, vol. 1, no. 1, 2013.
- [50] W. Hu, M. Fey, H. Ren, M. Nakata, Y. Dong, and J. Leskovec, "Ogb-lsc: A large-scale challenge for machine learning on graphs," *arXiv preprint arXiv:2103.09430*, 2021.
- [51] C. Edwards, C. Zhai, and H. Ji, "Text2Mol: Cross-modal molecule retrieval with natural language queries," in *Proceedings of the 2021 Conference on Empirical Methods in Natural Language Processing* (M.-F. Moens, X. Huang, L. Specia, and S. W.-t. Yih, eds.), (Online and Punta Cana, Dominican Republic), pp. 595–607, Association for Computational Linguistics, Nov. 2021.

- [52] T. Guo, B. Nan, Z. Liang, Z. Guo, N. Chawla, O. Wiest, X. Zhang, *et al.*, “What can large language models do in chemistry? a comprehensive benchmark on eight tasks,” *Advances in Neural Information Processing Systems*, vol. 36, pp. 59662–59688, 2023.
- [53] R. Taylor, M. Kardas, G. Cucurull, T. Scialom, A. Hartshorn, E. Saravia, A. Poulton, V. Kerkez, and R. Stojnic, “Galactica: A large language model for science,” *arXiv preprint arXiv:2211.09085*, 2022.
- [54] G. Helman, I. Shah, and G. Patlewicz, “Transitioning the generalised read-across approach (genra) to quantitative predictions: a case study using acute oral toxicity data,” *Computational Toxicology*, vol. 12, p. 100097, 2019.
- [55] C. Edwards, T. Lai, K. Ros, G. Honke, K. Cho, and H. Ji, “Translation between molecules and natural language,” 2022.
- [56] M. Krenn, Q. Ai, S. Barthel, N. Carson, A. Frei, N. C. Frey, P. Friederich, T. Gaudin, A. A. Gayle, K. M. Jablonka, *et al.*, “Selfies and the future of molecular string representations,” *Patterns*, vol. 3, no. 10, 2022.
- [57] T. Chen, S. Kornblith, M. Norouzi, and G. Hinton, “A simple framework for contrastive learning of visual representations,” in *International conference on machine learning*, pp. 1597–1607, PmlR, 2020.

Table of Contents

A	Limitations	15
B	Ethical considerations	15
C	Datasets: Additional Details	16
C.1	Model variants	16
C.2	Task and Datasets	17
D	Classification: Further Analysis and Discussion	18
D.1	Zero-Shot Evaluation	18
D.2	Effect of ICL Examples	18
D.3	Chain of Thought Prompting	21
D.4	Effect of Temperature	21
D.5	Impact of visual data	23
E	Regression: Further Analysis and Discussion	23
E.1	Effect of Finetuning	24
E.2	Effect of ICL Examples	25
E.3	Analysis of QM9 Multi-Target Prediction	25
F	Molecular Description: Further Analysis	25
F.1	Zero-Shot Evaluation	26
F.2	Effect of ICL Examples	26
F.3	Chain of Thought Prompting	27
G	Contrastive Learning for Vision Encoders	27
G.1	Augmentation-based contrastive learning	28
G.2	Tanimoto similarity-based contrastive learning	28
G.3	Overall loss function	28
H	Prompt Examples	30

In this supplementary material, we begin with important discussions on limitations (Section A) and ethical considerations (Section B). We have also included additional dataset details (Section C), comprehensive results and analysis for classification tasks (Section D), regression tasks (Section E), and molecular description tasks (Section F). Furthermore, we present our approach to contrastive learning for vision encoders (Section G) and provide detailed prompt examples (Section H) supporting our discussion in the main paper.

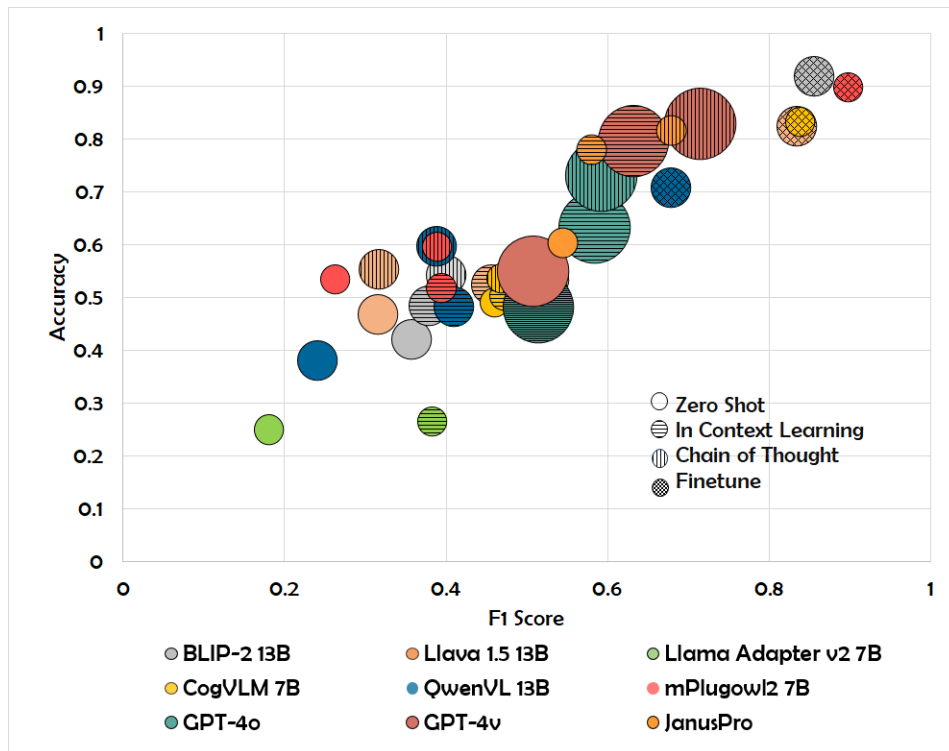


Figure 9: Performance comparison of Vision-Language Models (VLMs) across BACE, BBBP, HIV, Clintox, and Tox21 datasets, depicting Accuracy vs F1 Score. The bubble size represents the model's parameter scale

A Limitations

Here we discuss some of the limitations of our work.

Adaptation of closed-source models: Our efficient adaptation of large visual language models for molecular property prediction is limited to open-source models. Considering the strong performance of proprietary models in case of few-shot learning, it will be interesting to see how the capabilities of these closed-source models improve for this domain.

Advanced vision-language models: In our few-shot setup, we utilize an image representation of a molecule as additional input to the model. Since these models can take only one image as input, it was not possible to provide image representations for in-context examples as input. Future research could explore models capable of processing multiple images simultaneously.

B Ethical considerations

The integration of Vision-Language Models (VLMs) into molecular property prediction opens exciting new possibilities while also highlighting the importance of ethical considerations. By leveraging visual and textual representations, these models have the potential to accelerate discoveries in drug development and materials science in a more data-efficient manner. However, ensuring responsible AI development is crucial—focusing on model interpretability, fairness, and transparency

can enhance trust and reliability in scientific applications. Additionally, proactive measures, such as open benchmarking and ethical guidelines, can help steer this technology toward positive societal impact while mitigating risks. By addressing these considerations thoughtfully, VLMs can become a transformative tool for chemistry and beyond.

C Datasets: Additional Details

This study covers datasets with varied numbers of molecules, as low as 2k to as high as 3.7M. Figure 10 shows categorization of these datasets by tasks, Classification, Regression and Molecular Description. The default representation that is included with these datasets is SMILES and we generated the corresponding SELFIES representation and performed additional evaluations. All the data will be available on the provided link ¹.

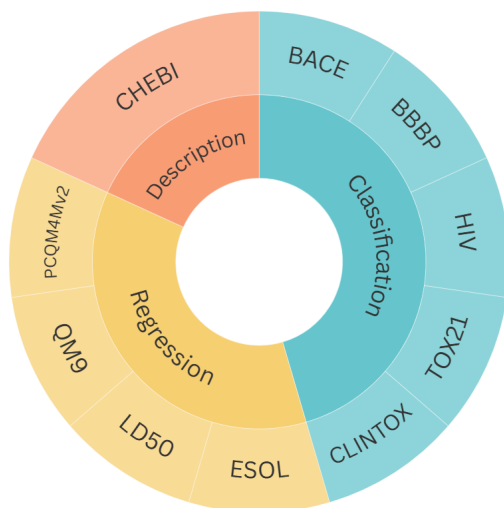


Figure 10: *Distribution of Datasets by Task Type*: The chart illustrates the categorization of datasets based on their primary task, either classification (blue) or regression (yellow).

C.1 Model variants

VLMs are evolved from LLMs that are designed to understand visual information and generate language based on both, textual and visual inputs. They integrate vision encoders and natural language processing techniques to interpret and describe images enabling use cases such as image captioning, visual question answering and multimodal translation. We study nine different state-of-the-art visual language models in this study.

Janus-Pro 7B: Janus-Pro 7B is a unified multimodal model that employs a novel decoupled visual encoding approach. It processes visual inputs differently for understanding versus generation tasks: using a SigLIP encoder to extract semantic features for understanding, while employing a VQ tokenizer for generation. These distinct visual representations are then mapped through separate adaptors into a shared input space, where a 7B-parameter autoregressive transformer processes the combined multimodal sequences.

BLIP-2: BLIP-2 (Bootstrapping Language-Image Pre-training) is a multimodal model developed by Salesforce that combines visual and language modalities to improve performance on tasks involving both visual inputs and textual information generation.

Llava 1.5: It is a multimodal model that integrates text and image data, excelling in tasks like Visual Question Answering (VQA), image captioning, and cross-modal retrieval. The model uses Vicuna v1.5 as the base LLM.

Llama Adapter V2: The LLaMA-Adapter V2 is an adaption technique that is intended to improve

¹Code and datasets available at: <https://molvision.github.io/MolVision/>

the LLaMA model’s ability to obey instructions while preserving parameter efficiency. It presents a number of important methods, such as early fusing of visual knowledge, joint training with discontinuous parameters, bias control of linear layers, and integration with expert models.

CogVLM: CogVLM is a vision-language model that integrates a Vision Transformer (ViT) encoder, MLP adapter, pretrained large language model, and a visual expert module. The ViT encoder uses the pretrained EVA2-CLIP-E model with the final layer removed for image feature compatibility.

QwenVL: Qwen-VL is a vision-language model for tasks like understanding, localization, and text reading. It consists of a visual encoder, a position-aware vision-language converter, and a large language model (Qwen-7B). The visual encoder, based on Openclip’s ViT-bigG, processes images by dividing them into patches.

mPlugOwl 2: mPLUGOWL2 integrates a vision encoder, visual abstractor, and language decoder for vision-language tasks. The ViT-L/14 encoder processes images into visual tokens, which the LLaMA-2-7B decoder converts into text.

GPT-4V: GPT-4V (GPT-4 with Vision) advances multimodal AI by processing both visual and textual inputs. Though its architecture is proprietary, GPT-4V excels in understanding and describing images, solving visual problems, and performing detailed visual-language reasoning across various domains.

GPT-4o: GPT-4o, OpenAI’s advanced language model, improves upon its predecessors with enhanced natural language processing, reasoning, and task completion. It offers better reliability, safety, and zero-shot generalization, though its architecture details remain largely undisclosed.

C.2 Task and Datasets

We utilize RDKit to generate molecular visualizations from SMILES structures. RDKit not only facilitates the conversion of SMILES strings into visual representations but also supports the transformation of SMILES into SELFIES strings. This functionality enables us to explore diverse molecular encoding techniques, thereby enhancing the robustness and adaptability of our predictive models. Since most existing datasets primarily feature SMILES strings, the ability to convert them to SELFIES representations extends the scope of our analysis. Each dataset contains a formatted prompt alongside the pathway to the visualized molecule image. Leveraging these datasets, we input the information into vision-language models for tasks such as visual question answering and instruction-based challenges. We use the following datasets in our benchmark.

BACE-V: The BACE-V dataset, adapted from the BACE (Binary Activity of Chemical Entities) dataset, provides 2D skeletal images of molecular structures along with key bioactivity data. Widely used for binary classification in bioactivity prediction, particularly for BACE-1 inhibitors linked to Alzheimer’s, the dataset includes both quantitative (IC50 values) and qualitative (binary) binding data. It features 154 BACE inhibitors for affinity prediction, 20 for pose prediction, and 34 for free energy prediction.

BBBP-V: The BBBP-V dataset, based on the Blood-Brain Barrier Penetration (BBBP) dataset, includes 2D skeletal images of molecular structures. It provides binary labels for BBB penetration (penetrant or non-penetrant) along with SMILES notations and key properties like molecular weight, lipophilicity (logP), and topological polar surface area (TPSA), all essential for predicting BBB permeability.

HIV-V: The HIV-V dataset, based on the HIV dataset, contains 2D skeletal images of molecular structures to support predictions of HIV replication inhibition. It includes binary labels for anti-HIV activity and key molecular parameters—molecular weight, logP, and TPSA—essential for assessing bioactivity and pharmacokinetics. Our evaluation focused on predicting HIV activity.

ClinTox-V: The ClinTox-V dataset, derived from the ClinTox dataset, includes 2D skeletal images of molecular structures to support predictions of clinical toxicity and FDA approval status. Represented by SMILES notation, each of the 1,491 compounds is labeled for toxicity or FDA approval, enabling two classification tasks. Our evaluation focused on predicting FDA approval status.

Tox21-V: The Tox21-V dataset, based on the Tox21 dataset, includes 2D skeletal molecular images for predicting chemical toxicity, critical for environmental and pharmaceutical safety. It contains hundreds of compounds, each represented by SMILES notation, with twelve binary labels from toxicological tests. Our evaluation focused on the NR-AR binary label.

ESOL-V: The ESOL-V dataset, based on the ESOL (Estimating Solubility of Organic Compounds in Water) dataset, includes 2D skeletal molecular images and key data for predicting aqueous solubility of organic compounds, crucial for drug development and environmental studies.

LD50-V: It is based on the LD50 (Lethal Dose 50) dataset and includes 2D skeletal molecular images and data on acute toxicity. It focuses on the dose required to cause death in 50% of test subjects, a key metric for safety assessment in drug development and environmental health.

QM9-V: The QM9-V dataset, derived from the QM9 dataset, contains 2D skeletal representations of molecular structures in image format, alongside various quantum chemical properties. QM9 provides extensive data on 12 quantum mechanical properties, including the dipole moment, isotropic polarizability, electronic spatial extent, HOMO (Highest Occupied Molecular Orbital energy), LUMO (Lowest Unoccupied Molecular Orbital energy), and HOMO-LUMO gap, among others.

PCQM4Mv2-V: The PCQM4Mv2-V dataset, derived from the PCQM4Mv2 dataset, contains 2D skeletal molecular images paired with quantum property data. The dataset focuses on predicting the HOMO-LUMO gap, an essential quantum property that provides insights into a molecule’s chemical stability and reactivity.

ChEBI-V: The ChEBI-V dataset, derived from the ChEBI database, contains 2D skeletal representations of molecular structures in image format, alongside comprehensive biological and chemical annotations. ChEBI-V provides structured information including molecular names, functional classifications, physicochemical properties, and biological roles such as enzyme inhibitors, receptor agonists, and therapeutic agents, making it valuable for molecular description and biological function prediction tasks.

D Classification: Further Analysis and Discussion

In this section, we discuss Zero-shot evaluation, effect of number of examples used in ICL, chain of thought prompting, effect of temperature in model performance and impact of visual data for classification task. Figure 9 show performance comparison of different models.

D.1 Zero-Shot Evaluation

We have included more detailed results with Zero-shot performance (Table 9 and 10) where we only ask questions with general outline to the models without using any in-context examples.

Table 9: **Zero-shot with SMILES:** The table shows variation in the F1-score & accuracy of different models when subjected to zero-shot prompting. In this evaluation, only the basic instruction is provided to the models to predict whether a given molecule string is toxic or not, without any additional context or examples.

Model	BACE-V	BBBP-V	HIV-V	Clintox-V	Tox21-V
JanusPro 7B	0.45(0.37)	0.42(0.44)	0.52(0.32)	0.31(0.32)	0.44(0.34)
BLIP2	0.28 (0.29)	0.31 (0.29)	0.42 (0.33)	0.29 (0.28)	0.42 (0.31)
Llava 1.5	0.37 (0.54)	0.43 (0.46)	0.38 (0.35)	0.36 (0.39)	0.46 (0.39)
Llama	0.34 (0.39)	0.41 (0.28)	0.21 (0.33)	0.28 (0.31)	0.12 (0.13)
CogVLM	0.27 (0.34)	0.31 (0.32)	0.22 (0.25)	0.47 (0.49)	0.17 (0.12)
QwenVLM	0.32 (0.39)	0.29 (0.12)	0.22 (0.29)	0.22 (0.15)	0.45 (0.37)
mPlugowl2	0.39 (0.38)	0.32 (0.31)	0.41 (0.27)	0.27 (0.26)	0.67 (0.13)

SMILES vs SELFIES: We examine and compare Zero-shot performance of models with SMILES and SELFIES representations. SELFIES generally yield better performance however on HIV dataset we see comparatively better performance with SMILES representation as shown in Tables 9 and 10. We also performed this analysis with ICL and has been discussed later.

D.2 Effect of ICL Examples

We conducted a comprehensive analysis of effects of number of examples ($k = 0, 2, 4$) in in-context learning (ICL) across vision-language models for molecular property prediction. More context does

Table 10: **Zero-shot performance with SELFIES**: The table illustrates the variation in the Accuracy (F1-score) of different models when subjected to zero-shot prompting. In this evaluation, only the basic instruction is provided to the models to predict whether a given molecule string is toxic or not, without any additional context or examples.

Model	BACE-V	BBBP-V	HIV-V	ClinTox-V	Tox21-V
JanusPro 7B	0.48(0.53)	0.54(0.581)	0.43 (0.36)	0.48 (0.37)	0.47 (0.31)
BLIP2	0.41 (0.34)	0.46 (0.48)	0.31 (0.29)	0.45 (0.47)	0.57 (0.21)
Llava 1.5	0.42 (0.48)	0.48 (0.50)	0.24 (0.33)	0.54 (0.64)	0.59 (0.15)
Llama Adapter v2 7B	0.42 (0.51)	0.39 (0.42)	0.21 (0.33)	0.41 (0.53)	0.14 (0.12)
CogVLM	0.42 (0.49)	0.49 (0.62)	0.28 (0.39)	0.44 (0.35)	0.16 (0.11)
QwenVL	0.42 (0.59)	0.41 (0.58)	0.21 (0.31)	0.16 (0.14)	0.16 (0.11)
mPlugOwl2	0.47 (0.25)	0.35 (0.23)	0.39 (0.28)	0.28 (0.22)	0.37 (0.17)

not always yield better results (Table 11, 12). The effectiveness of ICL varies significantly across datasets, as evidenced by CogVLM’s substantial improvement on ClinTox-V when increasing from $k = 0$ to $k = 4$ (0.54 to 0.76 accuracy). We also observed similar behaviours with CogVLM using SELFIES in Table 14. Different models demonstrate varying sensitivity to ICL, BLIP-2 however show consistent improvement with increased context, achieving its best performance with $k = 4$ across most datasets (Table 13).

Model QwenVL shows peak performance with $k = 2$ on several datasets (Table 17). Comparing SMILES representations (Table 11, 12) versus SELFIES representations (Table 15, 16,17 18, 19), SELFIES maintains more stable performance across different k values, particularly for complex models like mPlugOwl2 and CogVLM. These findings indicate that ICL’s effectiveness depends heavily on model architecture, molecular representation, and dataset characteristics.

We also included results with increased in-context examples with gpt-4o. With the exception of BBBP-V accuracy improved across all datasets with an increase in the number of in-context examples (k) to six or eight. Notably, on the BACE-V, and Clintox-V datasets, we observed approximately a 40% increase in accuracy. With the exception of BACE-V, the F1-score was also highest at $k=2$ or 4 across all datasets (Table 20).

Table 11: **Role of in-context examples**: ICL with $k = 0$ showing Accuracy (F1-score) of various models on different datasets with SMILES representations.

Model	BACE-V	BBBP-V	HIV-V	ClinTox-V	Tox21-V
JanusPro 7B	0.65(0.68)	0.52(0.51)	0.92(0.68)	0.41(0.31)	0.52(0.44)
BLIP2	0.36 (0.52)	0.33 (0.27)	0.41 (0.36)	0.37 (0.28)	0.63 (0.29)
Llava 1.5	0.55 (0.18)	0.47 (0.43)	0.35 (0.32)	0.33 (0.33)	0.64 (0.11)
Llama	0.39 (0.59)	0.36 (0.42)	0.21 (0.33)	0.22 (0.19)	0.15 (0.19)
CogVLM	0.39 (0.56)	0.48 (0.48)	0.39 (0.26)	0.54 (0.54)	0.65 (0.11)
QwenVLM	0.41 (0.52)	0.31 (0.11)	0.28 (0.21)	0.38 (0.12)	0.52 (0.43)
mPlugowl2	0.48 (0.16)	0.41 (0.43)	0.65 (0.18)	0.28 (0.28)	0.85 (0.11)

Table 12: **Effect of in-context examples**: ICL with $k = 4$ showing Accuracy (F1-score) of various models on different datasets with SMILES Representation.

Model	BACE-V	BBBP-V	HIV-V	ClinTox-V	Tox21-V
JanusPro 7B	0.73(0.62)	0.63(0.601))	0.95(0.69)	0.97(0.64)	0.71(0.62)
BLIP2	0.29 (0.42)	0.19 (0.11)	0.52 (0.32)	0.34 (0.36)	0.55 (0.39)
Llava 1.5	0.48 (0.38)	0.57 (0.66)	0.32 (0.33)	0.25 (0.22)	0.64 (0.25)
Llama	0.39 (0.56)	0.37 (0.22)	0.21 (0.33)	0.32 (0.19)	0.28 (0.12)
CogVLM	0.39 (0.54)	0.64 (0.34)	0.39 (0.26)	0.68 (0.48)	0.19 (0.11)
QwenVLM	0.42 (0.52)	0.31 (0.11)	0.42 (0.54)	0.81 (0.12)	0.72 (0.17)
mPlugowl2	0.58 (0.42)	0.43 (0.38)	0.71 (0.25)	0.38 (0.42)	0.83 (0.13)

Table 13: *Effect of in-context examples*: Accuracy (F1-score) of BLIP-2 Model using SELFIES representations with variation in number of in-context examples used in the prompt (k = 0, 2, 4).

Variation	BACE-V	BBBP-V	HIV-V	ClinTox-V	Tox21-V
k = 0	0.43(0.26)	0.38(0.27)	0.54(0.32)	0.33(0.42)	0.52(0.21)
k = 2	0.36(0.52)	0.37(0.29)	0.60(0.29)	0.34(0.36)	0.75(0.42)
k = 4	0.61 (0.27)	0.39 (0.31)	0.81 (0.39)	0.36 (0.44)	0.79 (0.48)

Table 14: *Impact of number of in-context examples*: The table illustrates the variation in the performance of the CogVLM model with ICL in terms of Accuracy (F1-score), which utilizes the Vicuna 7B as its backbone, when tested on the SELFIE representation of various datasets. The performance is evaluated with different numbers of in-context examples (k = 0, 2, 4) provided in the prompt. The following results are produced with temperature set to 0.

Variation	BACE-V	BBBP-V	HIV-V	ClinTox-V	Tox21-V
k = 0	0.34 (0.51)	0.36 (0.32)	0.24 (0.33)	0.54 (0.65)	0.26 (0.15)
k = 2	0.62 (0.44)	0.51 (0.58)	0.25 (0.29)	0.32 (0.37)	0.18 (0.14)
k = 4	0.44 (0.53)	0.38 (0.45)	0.32 (0.31)	0.76 (0.86)	0.47 (0.13)

Table 15: *Impact of number of in-context examples*: The table illustrates the variation in the performance of the Llava 1.5 model with ICL in terms of Accuracy (F1-score) using Llava 1.5 13 billion parameters, when tested on the SELFIE representation of various datasets. The performance is evaluated with different numbers of in-context examples (k = 0, 2, 4) provided in the prompt. (Temperature=0).

Variation	BACE-V	BBBP-V	HIV-V	ClinTox-V	Tox21-V
k = 0	0.62 (0.24)	0.35 (0.17)	0.51 (0.13)	0.20 (0.14)	0.76 (0.17)
k = 2	0.61 (0.33)	0.73 (0.46)	0.32 (0.35)	0.35 (0.36)	0.67 (0.47)
k = 4	0.49 (0.38)	0.56 (0.29)	0.42 (0.33)	0.25 (0.19)	0.89 (0.11)

Table 16: *Impact of number of in-context examples*: The table illustrates the variation in the performance of the mPlugOwl2 model with ICL in terms of Accuracy (F1-score). This model utilizes Llama2 7B as its backbone and is tested on the SELFIE representation of various datasets. The performance is evaluated with different numbers of in-context examples (k = 0, 2, 4) provided in the prompt. (Temperature = 0).

Variation	BACE-V	BBBP-V	HIV-V	ClinTox-V	Tox21-V
k = 0	0.53 (0.22)	0.48 (0.52)	0.57 (0.19)	0.22 (0.15)	0.62 (0.17)
k = 2	0.64 (0.65)	0.46 (0.46)	0.76 (0.74)	0.39 (0.43)	0.74 (0.21)
k = 4	0.61 (0.31)	0.35 (0.36)	0.73 (0.41)	0.46 (0.57)	0.76 (0.14)

Table 17: *Impact of number of in-context examples*: The table illustrates the variation in the performance of the QwenVL model with ICL in terms of Accuracy (F1-score) using QwenVL 7 B parameters, when tested on the SELFIE representation of various datasets. The performance is evaluated with different numbers of in-context examples (k = 0, 2, 4) provided in the prompt.(Temperature=0).

Variation	BACE-V	BBBP-V	HIV-V	ClinTox-V	Tox21-V
k = 0	0.41 (0.52)	0.31 (0.10)	0.80 (0.11)	0.18 (0.12)	0.52 (0.14)
k = 2	0.45 (0.38)	0.63 (0.49)	0.79 (0.49)	0.50 (0.48)	0.78 (0.76)
k = 4	0.42 (0.51)	0.29 (0.09)	0.81 (0.10)	0.42 (0.54)	0.72 (0.17)

Table 18: *Impact of number of in-context examples* The table illustrates the variation in the Accuracy (F1-score) of the ICL model using Llama Adapter V2, which utilizes Llama2 7B as its backbone, when tested on the SELFIE representation of various datasets. The performance is evaluated with different numbers of in-context examples (k = 0, 2, 4) provided in the prompt.(Temperature=0).

Variation	BACE-V	BBBP-V	HIV-V	ClinTox-V	Tox21-V
k = 0	0.37 (0.34)	0.49 (0.21)	0.21 (0.33)	0.30 (0.39)	0.14 (0.17)
k = 2	0.38 (0.44)	0.48 (0.23)	0.21 (0.37)	0.31 (0.35)	0.15 (0.17)
k = 4	0.36 (0.35)	0.51 (0.27)	0.31 (0.42)	0.50 (0.31)	0.15 (0.18)

Table 19: *Impact of number of in-context examples:* The table illustrates the variation in the Accuracy (F1-score) of the ICL model using the BLIP-2 model when tested on the SELFIE representation of various datasets. The performance is evaluated with different numbers of in-context examples (k = 0, 2, 4) provided in the prompt.(Temperature=0).

Variation	BACE-V	BBBP-V	HIV-V	Clintox-V	Tox21-V
k = 0	0.56 (0.10)	0.31 (0.12)	0.49 (0.24)	0.16 (0.09)	0.47 (0.32)
k = 2	0.61 (0.15)	0.35 (0.16)	0.56 (0.24)	0.18 (0.12)	0.41 (0.22)
k = 4	0.66 (0.26)	0.32 (0.11)	0.51 (0.29)	0.21 (0.10)	0.45 (0.19)

Table 20: **Effect of in-context examples:** Accuracy (F1-score) for different ICL examples on GPT-4o model.

ICL Variation	BACE-V	BBBP-V	HIV-V	Clintox-V	Tox21-V	Average
k=0	0.39 (0.55)	0.56 (0.64)	0.72 (0.53)	0.25 (0.33)	0.49 (0.46)	0.48/0.50
k=2	0.56 (0.53)	0.77 (0.81)	0.82 (0.56)	0.59 (0.44)	0.42 (0.58)	0.63/0.58
k=4	0.64 (0.52)	0.63 (0.66)	0.82 (0.78)	0.71 (0.69)	0.52 (0.44)	0.66/ 0.61
k=6	0.61 (0.48)	0.56 (0.62)	0.86 (0.79)	0.76 (0.63)	0.61 (0.43)	0.68/0.59
k=8	0.72 (0.51)	0.56 (0.60)	0.72 (0.64)	0.67 (0.69)	0.55 (0.34)	0.64/0.55
k=10	0.55 (0.35)	0.55 (0.59)	0.69 (0.23)	0.49 (0.53)	0.61 (0.27)	0.57/0.39

D.3 Chain of Thought Prompting

Table 21 demonstrates the effectiveness of Chain of Thought (CoT) prompting on molecular property classification tasks across five benchmark datasets. GPT-4v emerges as the top performer with an average accuracy of 72.32%, closely followed by GPT-4o at 71.14%, indicating that both commercial models excel when employing structured reasoning approaches. Janus achieves the third-highest performance with an average accuracy of 71.60%, demonstrating competitive capabilities among open-source models and particularly excelling on HIV-V (93.3%) and ClinTox-V (97.2%) datasets.

The results reveal significant performance variations across datasets, with HIV-V generally showing the highest accuracy scores across models, while BBBP-V and Tox21-V present greater challenges. Notably, QwenVLM shows strong performance on HIV-V (82.9%) and Tox21-V (73.9%), while mPlugOWL2 demonstrates exceptional performance on specific datasets like Tox21-V (76.0%) and HIV-V (75.2%). The remaining models exhibit moderate performance, with CogVLM achieving balanced results across datasets and BLIP-2 showing consistent but lower performance.

D.4 Effect of Temperature

The effect of temperature variation was shown in the main paper on one model (BLIP2 model) and here we include more results examining the effect of temperature variation under different settings (Table 24, 22 Table 27, and Table 26, 23, 25). We analyzed the impact of sampling temperature (ranging from 0.0 to 0.8) on model performance across different molecular representations and architectures. For SELFIES representation, the Llama Adapter v2 model shows optimal performance at moderate temperatures (0.2-0.4) for the BBBP-V dataset, achieving accuracy of 0.66 at temperature 0.2 (Table 23). SMILES representation exhibits different temperature sensitivity, with generally improved performance at higher temperatures across datasets (Table 24). BLIP2 demonstrates consistent improvement with increasing temperature, achieving peak average performance of 0.51

Table 21: *Classification Performance in Chain of Thought Prompting*: Comparisons of models evaluated on classification tasks across various datasets using Chain-of-Thought (CoT) prompting showing Accuracy (F1-score) with SMILES representations.

Model	BACE-V	BBBP-V	HIV-V	ClinTox-V	Tox21-V
GPT-4o	0.783(0.612)	0.696(0.481)	0.893(0.829)	0.683(0.582)	0.601(0.455)
GPT-4v	0.800(0.749)	0.716(0.620)	0.928(0.842)	0.972(0.729)	0.728(0.632)
BLIP-2	0.49 (0.52)	0.49 (0.41)	0.62 (0.32)	0.54 (0.36)	0.57 (0.39)
CogVLM	0.510(0.559)	0.673(0.396)	0.422(0.384)	0.650(0.701)	0.430(0.303)
mPlugOWL2	0.716(0.414)	0.555(0.362)	0.752 (0.413)	0.461(0.574)	0.76 (0.148)
Llava	0.523 (0.462)	0.582(0.493)	0.42 (0.33)	0.352(0.19)	0.893(0.11)
Llama-Adapter	0.430(0.339)	0.554(0.674)	0.429(0.312)	0.684(0.712)	0.437(0.382)
QwenVLM	0.528(0.429)	0.394(0.291)	0.829(0.329)	0.492(0.421)	0.739(0.471)
Janus	0.797(0.669)	0.696(0.661)	0.933(0.781)	0.972(0.729)	0.681(0.557)

at temperature 0.6 (Table 22). Llava 1.5 13B shows optimal performance at lower temperatures, particularly for the Tox21-V dataset with 0.93 accuracy at temperature 0.2 (Table 26). CogVLM exhibits more stable performance across temperature variations, with slight degradation at higher temperatures (Table 27). The mPlugOWL2 model achieves its best performance at temperature 0.2 across multiple datasets, notably reaching 0.88 accuracy on Tox21-V (Table 22). These findings suggest that moderate temperatures (0.2-0.4) generally provide optimal performance across models and representations, with specific optimal values being model and dataset dependent.

Table 22: **Effect of temperature**: Accuracy (F1-score) for different temperature settings using ICL (Samples k=2) on mPlugOWL2 model with SMILES.

Temp Variation	BACE-V	BBBP-V	HIV-V	Clintox-V	Tox21-V
0.0	0.59(0.32)	0.35(0.38)	0.62(0.30)	0.34(0.42)	0.69(0.57)
0.2	0.70 (0.28)	0.38(0.24)	0.74 (0.18)	0.78 (0.18)	0.88 (0.10)
0.4	0.65(0.15)	0.46 (0.46)	0.64(0.21)	0.30(0.36)	0.83(0.16)
0.6	0.60(0.23)	0.43(0.44)	0.62(0.26)	0.40(0.51)	0.73(0.16)
0.8	0.58(0.19)	0.41(0.43)	0.59(0.28)	0.43(0.52)	0.72(0.20)

Table 23: *Effect of temperature on SELFIE*: This table shows the performance of the Llama Adapter v2 model with ICL (k=2 examples) on various datasets represented in SELFIE notation.

Temp	BACE-V	BBBP-V	HIV-V	Clintox-V	Tox21-V
0.0	0.38 (0.44)	0.48 (0.23)	0.21 (0.37)	0.31 (0.35)	0.15 (0.17)
0.2	0.34 (0.51)	0.66 (0.79)	0.19 (0.31)	0.29 (0.88)	0.13 (0.18)
0.4	0.35 (0.49)	0.62 (0.75)	0.22 (0.32)	0.24 (0.85)	0.28 (0.11)
0.6	0.36 (0.43)	0.53 (0.68)	0.26 (0.33)	0.22 (0.83)	0.31 (0.18)
0.8	0.33 (0.44)	0.58 (0.69)	0.24 (0.39)	0.22 (0.81)	0.31 (0.15)

Table 24: *Effect of temperature on SMILES*: This table shows the performance of the Llama Adapter v2 model with ICL (k=2 examples) on various datasets represented in SMILES notation.

Temp	BACE-V	BBBP-V	HIV-V	Clintox-V	Tox21-V
0.0	0.28 (0.29)	0.18 (0.11)	0.19 (0.17)	0.29 (0.12)	0.31 (0.21)
0.2	0.38 (0.55)	0.22 (0.83)	0.21 (0.33)	0.28 (0.19)	0.32 (0.15)
0.4	0.35 (0.49)	0.35 (0.76)	0.42 (0.35)	0.22 (0.24)	0.39 (0.24)
0.6	0.39 (0.56)	0.23 (0.74)	0.31 (0.25)	0.31 (0.11)	0.41 (0.29)
0.8	0.43 (0.54)	0.29 (0.62)	0.37 (0.36)	0.26 (0.19)	0.41 (0.11)

Table 25: **Effect of Temperature on Model Performance:** Accuracy (F1-score) at different temperature settings using the BLIP2 model on various datasets. Higher temperatures generally show increased variability in F1-scores, with peak performance occurring at different temperature levels across datasets.

Temp Variation	BACE-V	BBBP-V	HIV-V	Clintox-V	Tox21-V	Average
0.0	0.33(0.42)	0.29(0.27)	0.56(0.24)	0.28(0.23)	0.65(0.32)	0.42(0.30)
0.2	0.35(0.49)	0.30(0.28)	0.56(0.30)	0.29(0.16)	0.69(0.34)	0.44(0.31)
0.4	0.34(0.42)	0.32(0.28)	0.59(0.27)	0.32(0.34)	0.72(0.34)	0.46(0.33)
0.6	0.41(0.54)	0.39(0.31)	0.64(0.35)	0.38(0.38)	0.72(0.36)	0.51(0.39)
0.8	0.38(0.48)	0.36(0.24)	0.62(0.32)	0.38(0.26)	0.78(0.44)	0.50(0.35)

Table 26: **Effect of temperature:** Performance analysis using the Llava 1.5 13B with ICL (k=2), focusing on diverse datasets represented in SELFIE format.

Temp	BACE-V	BBBP-V	HIV-V	Clintox-V	Tox21-V
0.0	0.61 (0.33)	0.73 (0.46)	0.32 (0.35)	0.35 (0.36)	0.67 (0.47)
0.2	0.59 (0.34)	0.63 (0.18)	0.36 (0.14)	0.19 (0.14)	0.93 (0.11)
0.4	0.57 (0.41)	0.34 (0.25)	0.34 (0.25)	0.31 (0.11)	0.86 (0.12)
0.6	0.48 (0.29)	0.42 (0.43)	0.36 (0.43)	0.34 (0.34)	0.77 (0.18)
0.8	0.52 (0.41)	0.37 (0.35)	0.30 (0.35)	0.36 (0.13)	0.75 (0.07)

Table 27: **Effect of temperature:** Analysis of temperature variation in various SELFIE based datasets with ICL (k=2) using CogVLM model.

Temp	BACE-V	BBBP-V	HIV-V	Clintox-V	Tox21-V
0.0	0.62 (0.44)	0.51 (0.58)	0.25 (0.29)	0.32 (0.37)	0.18 (0.14)
0.2	0.58 (0.41)	0.48 (0.54)	0.28 (0.52)	0.32 (0.31)	0.14 (0.35)
0.4	0.58 (0.41)	0.42 (0.52)	0.26 (0.48)	0.33 (0.33)	0.17 (0.34)
0.6	0.53 (0.44)	0.45 (0.48)	0.25 (0.42)	0.27 (0.31)	0.14 (0.32)
0.8	0.56 (0.39)	0.37 (0.39)	0.28 (0.49)	0.25 (0.30)	0.18 (0.32)

D.5 Impact of visual data

Table 28 underscores the stark contrast in performance between Llama 2, a large language model, and its VLM counterpart, Llama Adapter v2 after ICL. Llama Adapter v2 also show substantial improvement post-finetuning.

Table 28: **Impact of visual data:** First row shows Accuracy (F1-score) for ICL with language model Llama2, second row shows visual-language variant with improvement in performance, and third row demonstrates significant improvement in performance after finetuning.

Models	BACE-V	BBBP-V	HIV-V	ClinTox-V	Tox21-V
Llama 2 13B (ICL)	<0.01(<0.01)	0.05(0.04)	0.05(0.07)	0.05(0.08)	<0.01(<0.01)
Llama Adapter v2 7B (ICL)	0.28(0.29)	0.18(0.11)	0.19(0.17)	0.29(0.12)	0.31(0.21)
Llama Adapter v2 7B (LoRA)	0.52(0.48)	0.45(0.46)	0.43(0.42)	0.58(0.62)	0.68(0.69)

E Regression: Further Analysis and Discussion

The main paper presents the results of regression tasks on ESOL, LD50, QM9, and PCQM4Mv2 for in-context learning (ICL) with $k = 2$ and finetuning. Here we provide additional results for **zero-shot** learning, detailed in Table 30, and **few-shot** learning with $k = 4$, shown in Table 31. Figure 11 summarizes performance comparison across different models for regression tasks.

Furthermore, comprehensive evaluations on the QM9 dataset are included for 12 quantum mechanical targets under the **"all-together"** setting, where all targets are prompted simultaneously. These

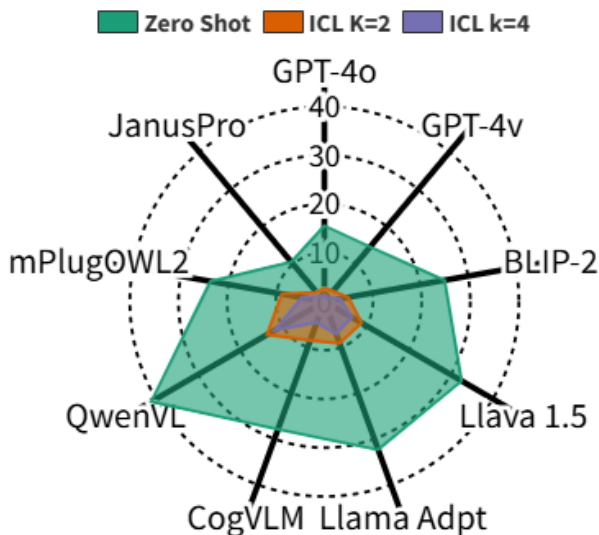


Figure 11: Radar plot comparing regression performance across various models (GPT-4v, GPT-4o, JansuPro, QwenVL, mPlugOWL2, BLIP-2, Llava 1.5 13B, CogVLM, and Llama Adapter v2 7B) averaged across ESOL, LD50, QM9, and PCQM4Mv2 datasets. The chart highlights Zero Shot (green) and Few Shot ($k=2$ in orange, $k=4$ in purple) capabilities.

evaluations cover zero-shot learning ($k = 0$), shown in Table 32; few-shot learning with $k = 2$, presented in Table 33; and few-shot learning with $k = 4$, detailed in Table 34.

E.1 Effect of Finetuning

The performance improvements achieved through LoRA-based finetuning are substantial across all regression tasks, as demonstrated in Table 29. BLIP-2 achieves the best overall performance with an average error of 1.925 across all datasets, excelling particularly on QM9-V (4.923 MAE) and PCQM4Mv2-V (0.235 MAE). CogVLM follows closely with an average error of 1.928, showing exceptional performance on ESOL-V with an RMSE of 1.102. Notably, Qwen VL demonstrates remarkable accuracy on LD50-V with a minimal MAE of 0.022. These finetuning results significantly outperform the in-context learning (ICL $k=2$) approaches presented in Table 3 of the main paper, where even the best-performing ICL model, Janus-Pro 7B, achieved only 2.52 average error. For example, BLIP-2’s finetuned performance (1.925 average error) represents a 61.5% improvement over its ICL performance (5.01 average error). Similarly, CogVLM improved from 8.50 to 1.928, and Qwen VL from 13.64 to 2.340. These dramatic improvements underscore the limitations of few-shot learning for molecular property prediction tasks and highlight the critical importance of task-specific parameter adaptation through finetuning.

Table 29: *Performance comparison after finetuning*: Regression tasks. Error comparison of models finetuned using LoRA across different datasets. The best performing models are highlighted with bold text. Second best model performance are underlined.

Model	ESOL-V (RMSE)	LD50-V (MAE)	QM9-V (MAE)	PCQM4Mv2-V (MAE)	Average
BLIP-2	1.764	0.779	4.923	0.235	1.925
Llava 1.5 13B	2.229	0.193	5.193	<u>0.602</u>	2.554
Llama Adapter v2 7B	4.032	0.624	7.921	<u>3.002</u>	3.895
CogVLM	1.102	0.592	5.221	0.795	<u>1.928</u>
Qwen VL	2.192	0.022	<u>5.021</u>	2.125	2.340
mPlugOWL2	<u>1.291</u>	<u>0.082</u>	8.029	1.621	2.756

E.2 Effect of ICL Examples

Tables 30 and 31 shows significant impact of in-context examples ($k=4$) versus zero-shot learning ($k=0$) across all models. GPT-4v maintains superior performance in both scenarios, ranking first with average metrics of 14.6485 and 1.04825 respectively, as shown in Table 30 and Table 31. The introduction of examples leads to substantial error reduction, exemplified by GPT-4v’s ESOL RMSE improving from 1.489 to 0.812, and its QM9 MAE decreasing from 45.296 to 2.503. Notably, the performance gap between models narrows with in-context examples, as evidenced by the reduction in average performance difference between best and worst models from 26.4815 (Table 30) to 10.69325 (Table 31), particularly in complex tasks like QM9 and PCQM4Mv2.

Table 30: *Performance comparison for zero-shot learning ($k=0$):* MAE, RMSE of Multimodal LLMs for molecular property prediction based regression tasks.

Model	ESOL (RMSE)	LD50 (MAE)	QM9 (MAE)	PCQM4Mv2 (MAE)	Average
GPT-4o	1.232	12.31	47.126	1.41	15.5195
GPT-4v	1.489	9.01	45.296	2.799	14.6485
JanusPro 7B	1.997	8.124	48.301	1.893	15.07875
BLIP-2	2.011	15.631	78.731	3.973	25.0865
Llava 1.5	18.198	14.952	93.182	3.967	32.57475
Llama Adapter	3.314	5.741	106.382	14.005	32.3605
CogVLM	2.093	23.769	80.766	4.939	27.89175
Qwen	4.119	24.388	116.353	19.66	41.13
mPlugOWL2	2.12	10.888	77.297	4.899	23.801

Table 31: *Performance comparison for few-shot learning ($k=4$):* MAE, RMSE of Multimodal LLMs for molecular property prediction based regression tasks.

Model	ESOL (RMSE)	LD50 (MAE)	QM9 (MAE)	PCQM4Mv2 (MAE)	Average
GPT-4o	0.867	0.614	3.147	0.222	1.2125
GPT-4v	0.812	0.686	2.503	0.192	1.048
JanusPro 7B	0.562	0.632	3.071	0.348	1.421
BLIP-2	1.289	0.696	10.339	0.882	3.3015
Llava 1.5	4.361	0.709	20.157	0.883	6.5275
Llama Adapter	2.309	2.431	19.840	3.809	7.09725
CogVLM	1.225	0.815	15.662	0.805	4.62675
Qwen	3.332	0.839	33.534	9.261	11.7415
mPlugOWL2	1.416	0.741	14.998	1.692	4.71175

E.3 Analysis of QM9 Multi-Target Prediction

Tables 32, 33, and 34 present the performance comparison for simultaneous prediction of all 12 QM9 molecular properties. In the zero-shot setting (Table 32), GPT-4o and GPT-4v demonstrate superior performance with average MAEs of 47.1264 and 45.2964 respectively. The addition of in-context examples ($k=2$, $k=4$) significantly improves prediction accuracy across all models, with GPT-4v achieving the best average MAE of 2.5028 at $k=4$. Notably, both GPT-4o and GPT-4v show consistent performance across different molecular properties, maintaining their superiority even in this challenging multi-target prediction scenario.

F Molecular Description: Further Analysis

We conducted a comprehensive evaluation of molecular description capabilities across multiple models and settings. This analysis examines zero-shot performance, the effects of in-context learning (ICL) with varying numbers of examples, and the impact of Chain of Thought (CoT) prompting on description quality. All experiments use the same evaluation metrics: BLEU-2, BLEU-4, ROUGE-1, ROUGE-2, ROUGE-L, and METEOR, with average scores reported for concise comparison.

Table 32: *Performance comparison for zero-shot learning (k=0)*: MAE of Multimodal LLMs for molecular property prediction based regression tasks on QM9 Dataset.

Model	QM9(Alpha)	QM9(Gap)	QM9(Homo)	QM9(Lummo)	QM9(Mu)	QM9(CV)	QM9(G298)	QM9(H298)	QM9(r2)	QM9(u298)	QM9(uf)	QM9(qpre)	QM9(Avg)
GPT-4o	11.0855	1.8364	1.0287	3.0245	2.6813	6.7424	85.0988	85.0906	195.5142	85.0902	85.0929	3.2317	47.1264
GPT-4v	14.925	2.4481	1.9924	2.129	3.129	6.1294	88.924	120.449	145.9812	66.2498	88.9192	2.2804	45.2964
JanusPro 7B	12.921	3.8238	1.8299	2.921	3.109	4.291	97.921	91.842	170.829	73.289	111.924	4.921	48.301
BLIP-2	47.902	3.920	2.220	2.844	11.294	59.201	122.842	129.912	255.901	102.120	194.201	12.422	78.7316
Llava 1.5	108.449	32.923	21.382	17.994	17.544	36.686	173.561	126.244	209.361	186.335	157.421	30.285	93.1821
Llama-Adapter	175.989	13.822	11.939	15.679	12.525	79.738	207.088	130.005	232.172	165.611	201.434	30.584	106.3822
CogVLM	93.191	2.119	1.4757	2.997	9.784	45.534	137.238	184.106	232.069	132.701	120.716	7.2616	80.7660
Qwen	184.191	8.201	7.772	9.009	46.111	137.302	240.019	129.090	220.322	172.828	197.466	43.923	116.3528
mPlugOWL2	72.706	3.676	4.280	2.457	5.673	31.363	157.058	157.078	214.541	100.495	121.920	56.315	77.2968

Table 33: *Performance comparison for few-shot learning (k=2)*: MAE of Multimodal LLMs for molecular property prediction based regression tasks on QM9 Dataset.

Model	QM9(Alpha)	QM9(Gap)	QM9(Homo)	QM9(Lummo)	QM9(Mu)	QM9(CV)	QM9(G298)	QM9(H298)	QM9(r2)	QM9(u298)	QM9(uf)	QM9(qpre)	QM9(Avg)
GPT-4o	2.32	0.2126	0.3113	0.2212	0.9787	0.857	17.9428	17.9434	22.948	17.9435	17.9432	0.9126	8.3779
GPT-4v	3.1	0.484	0.396	0.293	0.968	0.998	18.021	18.022	24.405	18.022	18.021	0.725	8.6217
JanusPro 7B	2.892	0.429	0.3329	0.3392	0.792	0.729	18.291	18.728	21.882	19.821	17.211	0.884	8.5276
BLIP-2	3.401	0.713	0.891	0.629	2.14	2.129	22.092	21.921	85.239	29.912	22.12	0.982	16.014
Llava 1.5	17.472	2.191	1.991	1.629	7.737	3.516	26.653	68.502	100.307	56.087	36.873	1.024	26.9985
Llama-adapter	17.316	1.621	2.091	1.032	4.554	5.011	39.585	45.626	130.37	58.654	29.255	2.02	28.0946
CogVLM	7.6465	0.91	1.012	0.876	3.613	2.799	21.292	27.702	174.554	45.178	23.74	0.822	25.8454
QwenVLM	13.563	2.03	1.293	1.075	10.587	3.563	130.992	75.385	134.581	55.007	36.941	2.036	38.9211
mPlugOWL2	10.336	1.832	1.432	1.71	2.685	3.233	23.091	37.263	189.806	52.405	27.379	0.829	29.333

Table 34: *Performance comparison for few-shot learning (k=4)*: MAE of Multimodal LLMs for molecular property prediction based regression tasks on QM9 Dataset.

Model	QM9(Alpha)	QM9(Gap)	QM9(Homo)	QM9(Lummo)	QM9(Mu)	QM9(CV)	QM9(G298)	QM9(H298)	QM9(r2)	QM9(u298)	QM9(uf)	QM9(qpre)	QM9(Avg)
GPT-4o	1.28	0.0184	0.0137	0.0053	0.2787	0.257	3.9572	3.9561	20.052	3.956	3.9563	0.0334	3.1470
GPT-4v	1.56	0.0244	0.0383	0.0069	0.9664	0.207	3.0218	3.0214	15.1194	3.0215	3.0215	0.0251	2.5028
JanusPro 7B	1.992	0.0892	0.0782	0.0098	0.389	0.108	5.208	4.592	17.229	4.092	2.981	0.0782	3.0705
BLIP-2	2.992	0.064	0.192	0.023	1.102	0.942	9.28	19.029	73.923	9.284	7.128	0.103	10.3385
CogVLM	6.9543	0.166	0.112	0.196	1.644	2.912	16.482	19.597	98.439	18.502	22.844	0.0919	15.6617
mPlugOWL2	8.823	1.016	1.011	1.489	1.556	2.746	14.191	22.711	88.797	15.687	21.826	0.126	14.9983
llava	10.064	0.362	0.221	0.092	1.76	3.014	21.824	65.123	80.81	28.139	30.044	0.426	20.1566
llama-adapter	15.961	1.129	1.071	0.902	2.65	4.741	25.978	27.412	93.616	37.095	26.511	1.019	19.8404
qwen	12.988	1.203	1.102	1.091	2.813	2.988	97.619	69.377	127.947	51.125	33.136	1.018	33.5339

F.1 Zero-Shot Evaluation

We conducted experiments evaluating molecular description capabilities in a zero-shot setting. GPT-4o demonstrates superior performance across all metrics, achieving the highest average score of 27.541 (Table 35). GPT-4v follows with a notable performance gap but consistent profile (24.556 average). Among the remaining models, JanusPro and Llava 1.5 13B form the second tier (19.642 and 18.140 average, respectively), followed by CogVLM and mPlugOWL2 showing comparable capabilities (16.158 and 16.004). BLIP-2 and Qwen VL deliver similar mid-to-low range performance, while Llama Adapter v2 7B struggles significantly with this task (10.048 average). These results suggest that general-purpose models with extensive pretraining currently maintain substantial advantages in zero-shot molecular understanding and description tasks.

F.2 Effect of ICL Examples

Tables 36 and 37 demonstrate significant performance improvements when increasing from 2-shot to 4-shot learning. GPT-4v leads in the 2-shot setting with the highest average score of 43.400, while GPT-4o achieves superior results in the 4-shot setting with an average of 59.727, showing a remarkable improvement of 17.6 percentage points over its 2-shot performance. All models exhibit

Table 35: *Molecular description performance in zero-shot setting*: Comparison of models evaluated on molecular description task without finetuning. The best performing models are highlighted with bold text.

Models	BLEU-2 \uparrow	BLEU-4 \uparrow	ROUGE-1 \uparrow	ROUGE-2 \uparrow	ROUGE-L \uparrow	METEOR \uparrow	Average \uparrow
GPT-4o	27.853	25.491	29.376	26.184	28.729	27.615	27.541
GPT-4v	24.837	23.492	25.876	24.184	25.329	23.615	24.556
BLIP-2	12.610	11.780	12.480	12.150	12.390	11.940	12.225
CogVLM	16.753	15.292	16.876	15.684	16.529	15.815	16.158
mPlugOWL2	16.621	15.220	16.432	15.837	16.286	15.629	16.004
Llava 1.5 13B	18.662	17.544	18.470	18.047	18.340	17.774	18.140
Llama Adapter v2 7B	10.332	9.723	10.235	9.985	10.173	9.841	10.048
Qwen VL	14.497	13.634	14.360	14.008	14.267	13.802	14.095
JanusPro	19.753	18.492	20.876	19.284	20.529	18.915	19.642

consistent gains when provided with additional examples, with larger models generally demonstrating better utilization of in-context examples. JanusPro maintains strong performance in both settings, while smaller models like Llama Adapter v2 7B show more modest improvements.

Table 36: *Molecular description performance in few-shot setting (k=2)*: Comparison of models evaluated on molecular description task with 2-shot learning. The best performing models are highlighted with bold text.

Models	BLEU-2 \uparrow	BLEU-4 \uparrow	ROUGE-1 \uparrow	ROUGE-2 \uparrow	ROUGE-L \uparrow	METEOR \uparrow	Average \uparrow
GPT-4o	43.330	40.180	42.870	42.070	42.670	41.740	42.143
GPT-4v	43.720	43.020	43.620	43.310	43.580	43.150	43.400
BLIP-2	30.265	29.273	30.136	29.719	30.032	29.546	29.829
CogVLM	31.951	30.552	31.762	31.167	31.616	30.959	31.335
mPlugOWL2	26.664	24.795	26.390	25.619	26.184	25.359	25.835
Llava 1.5 13B	29.818	28.617	29.653	29.137	29.526	28.951	29.284
Llama Adapter v2 7B	21.619	20.465	21.469	21.142	21.377	20.982	21.176
Qwen VL	31.062	29.051	30.817	29.923	30.600	29.583	30.173
JanusPro	38.286	37.061	38.153	37.618	38.021	37.262	37.734

Table 37: *Molecular description performance in few-shot setting (k=4)*: Comparison of models evaluated on molecular description task with 4-shot learning. The best performing models are highlighted with bold text.

Models	BLEU-2 \uparrow	BLEU-4 \uparrow	ROUGE-1 \uparrow	ROUGE-2 \uparrow	ROUGE-L \uparrow	METEOR \uparrow	Average \uparrow
GPT-4o	61.310	58.690	60.490	59.220	60.060	58.590	59.727
GPT-4v	55.780	54.430	55.580	54.930	55.460	54.650	55.138
BLIP-2	36.064	34.530	35.896	35.227	35.728	35.049	35.416
CogVLM	40.285	39.062	40.152	39.618	40.020	39.262	39.733
mPlugOWL2	33.774	32.299	33.614	32.969	33.454	32.792	33.150
Llava 1.5 13B	40.775	39.507	40.638	40.083	40.502	39.715	40.203
Llama Adapter v2 7B	32.063	31.075	31.947	31.456	31.857	31.298	31.616
Qwen VL	40.285	39.062	40.152	39.618	40.020	39.262	39.733
JanusPro	50.574	48.696	50.373	49.599	50.104	49.098	49.741

F.3 Chain of Thought Prompting

Table 38 illustrates the impact of Chain of Thought (CoT) prompting on molecular description tasks. GPT-4o achieves superior performance across all metrics with an average score of 61.494, slightly outperforming GPT-4v (59.549). Both models demonstrate strong capabilities when encouraged to reason step-by-step. JanusPro maintains its position as the third-best performer with an average score of 53.703, showing considerable potential among non-commercial models. The remaining models show varying degrees of effectiveness with CoT prompting, with Llava and CogVLM achieving similar performance (43.393 and 42.878, respectively). Notably, when compared to few-shot learning results, CoT prompting appears to further enhance model performance, particularly for larger models, suggesting that structured reasoning approaches are beneficial for molecular description tasks.

G Contrastive Learning for Vision Encoders

We explore two contrastive learning strategies for enhancing the vision encoder’s ability to capture molecular structural information: augmentation-based and Tanimoto similarity-based approaches.

Table 38: *Molecular description performance in Chain-of-thought setting*: Comparison of models evaluated on molecular description task with Chain of Thought (CoT). The best performing models are highlighted with bold text.

Models	BLEU-2 \uparrow	BLEU-4 \uparrow	ROUGE-1 \uparrow	ROUGE-2 \uparrow	ROUGE-L \uparrow	METEOR \uparrow	Average \uparrow
GPT-4o	62.162	60.743	62.406	61.151	62.006	60.495	61.494
GPT-4v	60.242	58.784	60.026	59.324	59.897	59.022	59.549
BLIP2	38.708	37.092	38.530	37.825	38.344	37.638	38.023
CogVLM	43.467	42.187	43.324	42.745	43.182	42.361	42.878
mPlugOWL	36.475	34.883	36.303	35.606	36.130	35.416	35.802
Llava	43.996	42.668	43.849	43.249	43.702	42.892	43.393
Llama Adapter	34.628	33.561	34.503	33.972	34.405	33.802	34.145
Qwen	43.387	42.187	43.324	42.745	43.182	42.403	42.871
Janus	54.571	52.591	54.352	53.567	54.112	53.026	53.703

This additional loss is used with LoRA finetuning. We experimente with BLIP-2 considering its better performance across all tasks. The motivation is to enable the vision encoder to learn more discriminative representations of molecular structures by leveraging either image transformations or chemical similarity relationships. The performance of these contrastive learning approaches across multiple molecular datasets is summarized in the main paper, while the detailed metrics on the molecular description task are presented in Table 39.

Table 39: *Molecular description performance using Contrastive Learning* Comparison of BLIP2 evaluated on molecular description task with Augmentation (Aug) and Tanimoto Augmentation (T-Aug).

Models	BLEU-2 \uparrow	BLEU-4 \uparrow	ROUGE-1 \uparrow	ROUGE-2 \uparrow	ROUGE-L \uparrow	METEOR \uparrow	Average \uparrow
Lora	59.062	58.034	58.933	58.466	58.889	58.185	58.595
Aug	61.530	60.307	61.398	60.863	61.266	60.507	60.979
T-Aug	64.176	63.192	64.072	63.641	63.966	63.352	63.733

G.1 Augmentation-based contrastive learning

We generate multiple views of the same molecule using a set of image transformations including rotations (at angles 45°, 90°, 135°, 180°, 225°, 270°, and 315°), vertical and horizontal flips, solarization, posterization, and auto-contrast adjustments. For each molecule image, we randomly apply two transformations to create positive pairs for contrastive learning.

Figure 12 illustrates the analysis of our augmentation-based approach through t-SNE visualizations of the visual encodings. While our main paper demonstrates the superior performance of contrastive learning using Tanimoto similarity, here we present results from image augmentation techniques for comparison. The left plot shows the visual encodings from BLIP-2 before cross-modal fusion, with clusters exhibiting significant overlap. The right plot displays the representations after cross-modal fusion, where the clusters become more distinguishable but still less defined than those achieved with Tanimoto similarity methods discussed in the main paper. This comparative analysis confirms that Tanimoto similarity-based approaches provide better molecular structure differentiation than augmentation-based techniques alone, particularly for chemical structure representation tasks.

G.2 Tanimoto similarity-based contrastive learning

Rather than using augmented views, we leverage chemical similarity to define positive pairs. For each molecule, we identify three structurally similar molecules with Tanimoto similarity scores >0.85 to serve as positive examples. This approach ensures that the model learns from meaningful chemical relationships rather than artificial transformations.

G.3 Overall loss function

For both approaches, we implement a contrastive loss based on NT-Xent (Normalized Temperature-scaled Cross Entropy) as used in SimCLR. The fundamental principle behind this loss function is to learn discriminative molecular representations by pulling together embeddings of similar molecules

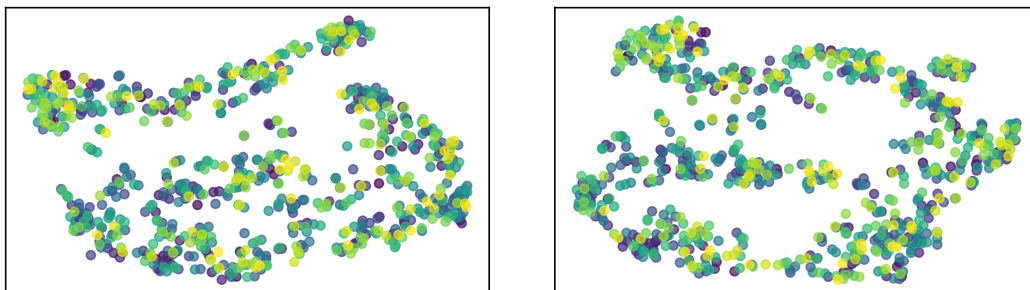


Figure 12: **Analyzing visual features:** The two plots show t-SNE visualizations of visual encodings of BLIP-2 before and after cross-modal fusion respectively using augmentative technique.

(positive pairs) while pushing apart embeddings of dissimilar molecules (negative pairs) in the representation space.

The contrastive loss is mathematically defined as:

$$\mathcal{L}_{\text{contrastive}} = -\frac{1}{2N} \sum_{i=1}^N \log \frac{\exp(\text{sim}(z_i, z_j)/\tau)}{\sum_{k=1}^{2N} \mathbf{1}_{[k \neq i]} \exp(\text{sim}(z_i, z_k)/\tau)} \quad (1)$$

The key components of this formulation include z_i and z_j , which represent the normalized embeddings of a positive pair obtained from the vision encoder after processing molecular images. The similarity function $\text{sim}(z_i, z_j) = \frac{z_i^T z_j}{\|z_i\| \|z_j\|}$ denotes the cosine similarity between two embeddings, while $\tau = 0.5$ is the temperature parameter that controls the concentration of the distribution around positive pairs. The batch size is represented by N , resulting in $2N$ total samples when considering both elements of each positive pair, and $\mathbf{1}_{[k \neq i]}$ is an indicator function that excludes the case where $k = i$ to prevent self-comparison.

The loss function operates by computing the probability that embedding z_i is most similar to its positive counterpart z_j compared to all other embeddings in the batch. The numerator $\exp(\text{sim}(z_i, z_j)/\tau)$ represents the similarity between the positive pair, while the denominator sums over all possible negative pairs within the batch, creating a softmax-like normalization that encourages the model to distinguish between related and unrelated molecular structures.

The temperature parameter τ plays a crucial role in controlling the learning dynamics. A lower temperature such as our chosen value of 0.5 creates sharper distributions, making the model more sensitive to small differences in similarity scores and encouraging tighter clustering of positive pairs. This helps the encoder learn more discriminative features that are essential for downstream molecular property prediction across classification tasks, regression tasks, and molecular description tasks.

During training, this contrastive loss is combined with the task-specific loss for the target dataset:

$$\mathcal{L}_{\text{total}} = \mathcal{L}_{\text{task}} + \lambda \mathcal{L}_{\text{contrastive}} \quad (2)$$

Here, $\mathcal{L}_{\text{task}}$ represents the primary loss for the specific molecular property prediction task, which varies depending on whether we are performing classification (cross-entropy loss), regression (mean squared error or mean absolute error), or molecular description (sequence generation loss). The weighting parameter λ balances the contribution of the contrastive learning objective with the task-specific objective. This combined loss function is optimized during LoRA finetuning, allowing the vision encoder to simultaneously learn task-specific features for classification, regression, and molecular description tasks while maintaining the ability to distinguish between different molecular structures through contrastive learning. The integration of contrastive learning with task-specific objectives enables the model to develop robust molecular representations that generalize well across diverse downstream applications in molecular property prediction.

H Prompt Examples

In this section, we show some prompt examples as used for various datasets. We have included some example ICL prompts specific to some of the dataset (Figure 13, 16, 14, 17,15). For regression tasks, we demonstrate an example using the ESOL dataset for solubility prediction (Figure 19). With ICL $k=0$ (different from zero-shot), we have all other section as shown in the prompt, however the example block is not used as input. The additional information as available with task instruction differentiates it from zero-shot, as models do not see ‘Task instruction’ in zero-shot. Prompt examples for ICL are included with SELFIES representations (Figure 18).

We include a chain-of-thought prompt example for the BBBP dataset (Figure 21), showing the step-by-step reasoning approach for classification tasks.

We provide a prompt example for molecular description tasks using the ChEBI dataset with ICL $k=2$ (Figure 20), demonstrating how the model generates natural language descriptions of molecular structures and properties.



} Image Prompt

You are an expert chemist, your task is to predict the property of molecule using your experienced chemical property prediction knowledge.

} General Outline

Please strictly follow the format, no other information can be provided. Given the SMILES string of a molecule, predict the molecular properties of a given chemical compound based on its structure, by analyzing whether it can inhibit(Yes) the Beta-site Amyloid Precursor Protein Cleaving Enzyme 1 (BACE1) or cannot inhibit(No) BACE1. Consider factors such as molecular weight, atom count, bond types, and functional groups in order to assess the compound's drug-likeness and its potential to serve as an effective therapeutic agent for Alzheimer's disease, please answer with only Yes or No. A few examples are provided in the beginning.

} Task Instruction

SMILES:
O1CCOc2c1cc(cc2)C1(N=C(N)N(C)C1=O)c1cc(ccc1)-c1cccnc1
 BACE-1 Inhibit: Yes
 SMILES:
OC(C(NC(=O)c1c2ccnc2n(c1)C(=O)N(CCCC)C)Cc1ccccc1)C[NH2+]C1CC1
 BACE-1 Inhibit: No

} Examples

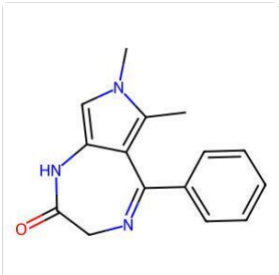
Below is the molecule whose property you have to predict. Along with is the image structure of the molecule.
 SMILES: O=C1N(C)C(=NC(=C1)[C@H]1C[C@H]1c1ccccc1)N
 BACE-1 Inhibit:
 You have to predict whether it has Penetration with answer Yes or No only.

} Question

No

} Answer

Figure 13: *Sample prompt for BACE-V*: A general outline is provided at first followed by set of instructions to be more specific about the task. The task is explained briefly and expected output is stated. In our case it should be Yes/No. This includes ICL examples with k=2 (No of samples). With this the main question is asked. The chemical compound whose property is to be expected is represented in its molecular structure created using RDKit which goes along with the text input.



} Image Prompt

You are an expert chemist, your task is to predict the property of molecule using your experienced chemical property prediction knowledge.

} General Outline

Please strictly follow the format, no other information can be provided. Given the SMILES string of a molecule, the task focuses on predicting molecular properties, specifically penetration/non-penetration to the brain-blood barrier, based on the SMILES string representation of each molecule. You will be provided with several examples molecules, each accompanied by a binary label indicating whether it has penetrative property (Yes) or not (No). Please answer with only Yes or No.

} Task Instruction

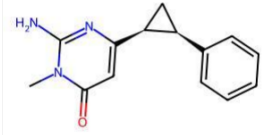
SMILES: O=C1Nc2ccccc2N1C3CCN(CCOc4ccccc4)CC3
 Penetration: Yes
 SMILES:
CC1CN(CCN1)c2cc3N(C=C(C(O)=O)C(=O)c3c(C)c2F)C4CC4
 Penetration: No

} Examples

Below is the molecule who's property you have to predict. Along with is the image structure of the molecule.
 SMILES:
C1=C2C(=C([N]1C)C)C(=NCC(N2)=O)C3=CC=CC=C3
 Penetration:
 You have to predict whether it has Penetration with answer Yes or No only.

} Question

Figure 14: **Example prompt:** The figure presents a task designed for predicting molecular properties, specifically penetration through the blood-brain barrier (BBBP-V dataset), using the SMILES string representation. The general outline and specific instructions detail the expected binary output (Yes/No). Two example molecules are provided to illustrate the task, followed by the main question, which includes the SMILES string and structure of the target molecule, generated with RDKit.



}

Image Prompt

You are an expert chemist, your task is to predict the property of molecule using your experienced chemical property prediction knowledge.

}

General Outline

Please strictly follow the format, no other information can be provided. Given the SMILES string of a molecule, predict the molecular properties of a given chemical compound based on its structure, by analyzing whether it can inhibit(Yes) the Beta-site Amyloid Precursor Protein Cleaving Enzyme 1 (BACE1) or cannot inhibit(No) BACE1. Consider factors such as molecular weight, atom count, bond types, and functional groups in order to assess the compound's drug-likeness and its potential to serve as an effective therapeutic agent for Alzheimer's disease, please answer with only Yes or No. A few examples are provided in the beginning.

}

Task Instruction

SMILES:
O1CCOc2c1cc(cc2)C1(N=C(N)N(C)C1=O)c1cc(ccc1)-c1ccnc1
 BACE-1 Inhibit: Yes
 SMILES:
OC(C(NC(=O)c1c2ccnc2n(c1)C(=O)N(CCCC)C)Cc1ccccc1)C[NH2+]C1CC1
 BACE-1 Inhibit: No

}

Examples

Below is the molecule whose property you have to predict. Along with is the image structure of the molecule.
 SMILES: O=C1N(C)C(=NC(=C1)[C@H]1C[C@H]1c1ccccc1)N
 BACE-1 Inhibit:
 You have to predict whether it has Penetration with answer Yes or No only.

}

Question

No

}

Answer

Figure 15: **Example prompt:** The figure outlines a task for predicting the ability of molecules to inhibit HIV replication (HIV-V dataset), based on their SMILES string representation. The general outline and specific instructions require a binary output (Yes/No). Example molecules are provided to illustrate the task, followed by the main question, which includes the SMILES string and structure of the target molecule, generated with RDKit.

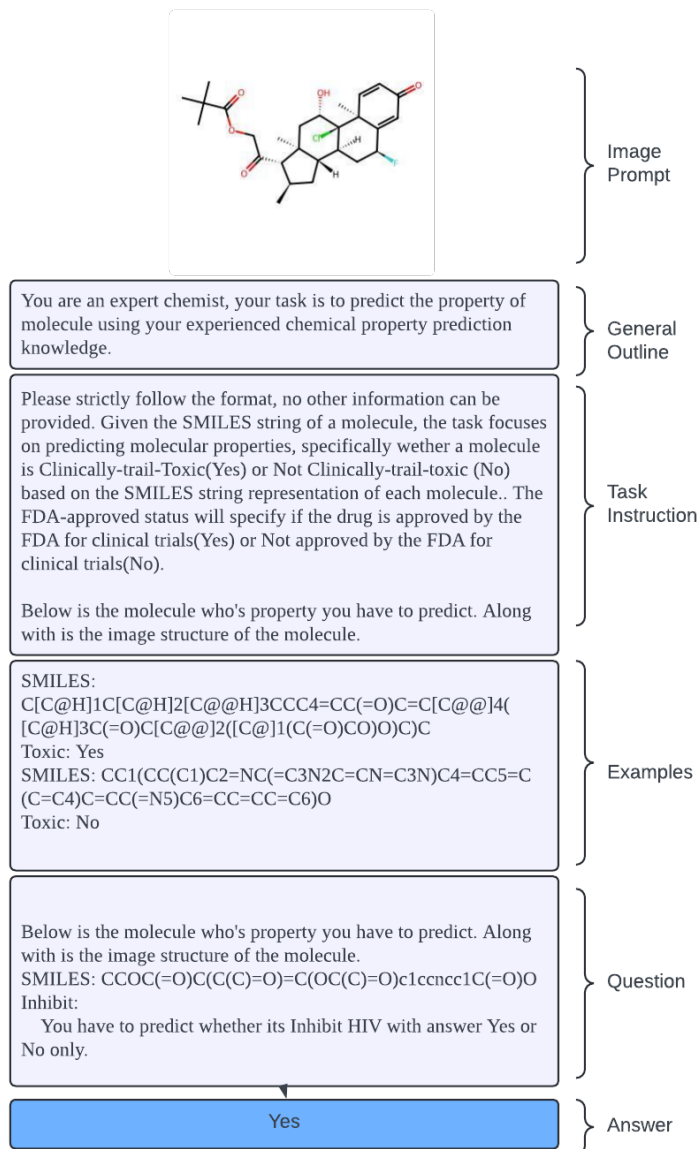


Figure 16: **Example prompt:** The figure outlines a task for predicting whether molecules are clinically trial-toxic (ClinTox-V dataset), using their SMILES string representation. The general outline and specific instructions require a binary output (Yes/No) to indicate if the molecule is approved by the FDA for clinical trials. Example molecules are provided to illustrate the task, followed by the main question, which includes the SMILES string and structure of the target molecule, generated with RDKit.

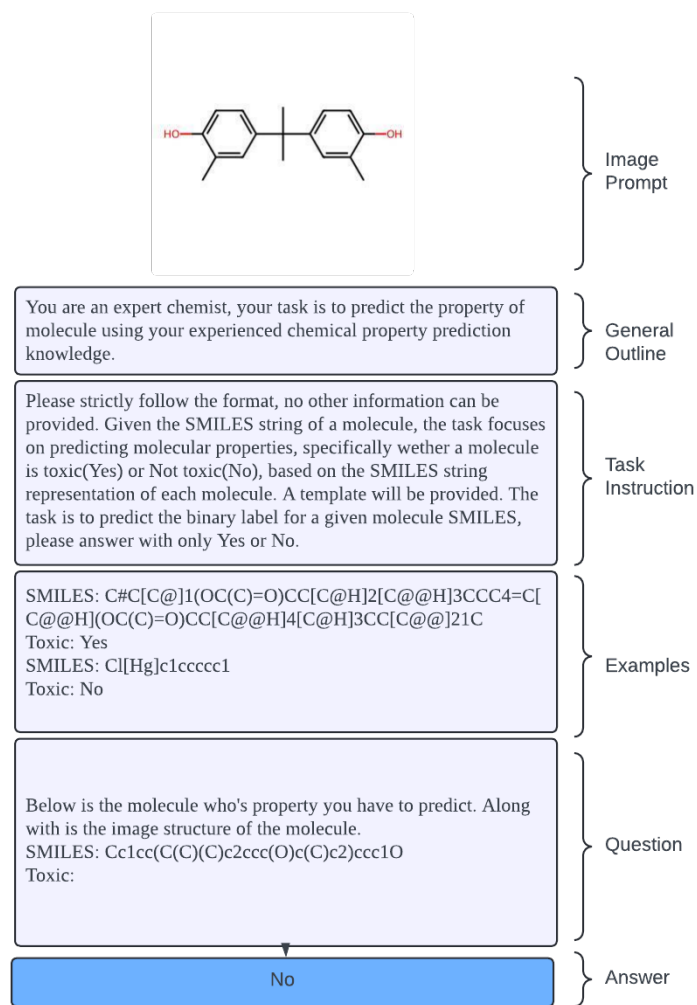


Figure 17: **Example prompt:** The figure outlines a task for predicting the toxicity of molecules based on their SMILES string representation, specifically in the context of the Tox21 dataset. The general outline and specific instructions require a binary output (Yes/No) to indicate the molecule's toxicity. Example molecules are provided to illustrate the task, followed by the main question, which includes the SMILES string and structure of the target molecule, generated with RDKit.

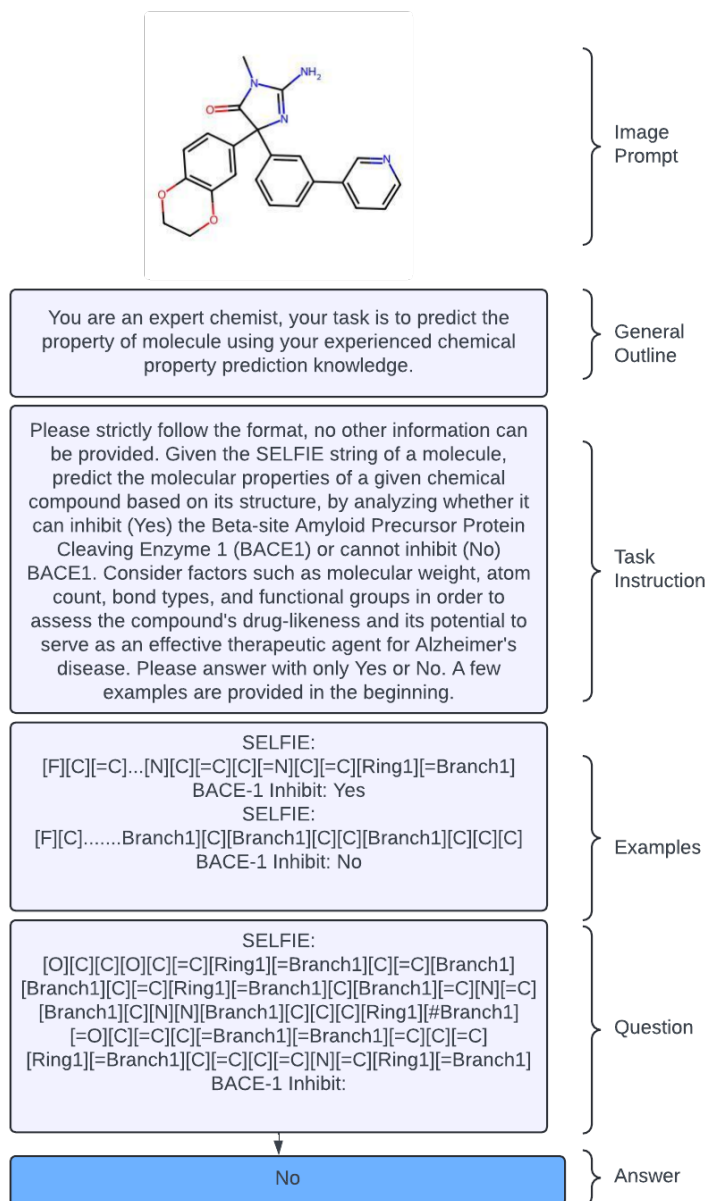


Figure 18: **Example prompt:** The figure outlines a task for predicting the ability of molecules for BACE-Inhibit (BACE-V dataset), using their SELFIES string representation. The general outline and specific instructions require a binary output (Yes/No). Example molecules are provided to illustrate the task, followed by the main question, which includes the SELFIES string and structure of the target molecule, generated with RDKit.

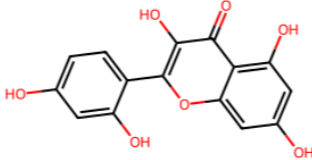


Image Prompt

General Outline

As an expert chemist specializing in molecular property prediction, your task is to accurately estimate the measured log solubility in mols per litre for various compounds.

Task Instruction

Please strictly follow the format, no other information can be provided. Given the Smiles string of a molecule, predict the molecular properties of a given chemical compound based on its structure. You have extensive knowledge of chemical structures, solubility principles, and structure-property relationships. Consider the following information about the molecule: its molecular weight is 302.2380000000006 g/mol, and it has 5 H-bond donors. Using your expertise, analyze the given Smiles representation of the molecule, considering factors such as polarity, molecular weight, H-bond donors, and other functional groups that influence solubility. Based on this analysis, provide your best prediction of the measured log solubility in mols per litre for the following Smiles string: Oc1ccc(c(O)c1)c3oc2cc(O)cc(O)c2c(=O)c3O. You don't need any extra information for this task. Your task is to predict the answer only. The predicted output should only be a number of log solubility in mols per litre.

Examples

Smiles: Nc1ccccc1Cl Log Solubility: -1.52
 Smiles: Oc1ccccc1 Log Solubility: -2.54

Question

Below is the molecule who's property you have to predict. Along with is the image structure of the molecule.
 Smiles: Oc1ccc(c(O)c1)c3oc2cc(O)cc(O)c2c(=O)c3O Log Solubility:

Answer

-3.083

Figure 19: **Example prompt:** The figure outlines a task for predicting the log solubility of molecules based on their SMILES string representation, using the ESOL dataset. The general outline and specific instructions require a numerical output for log solubility in mols per litre. Two example molecules ($k=2$) are provided to illustrate the task, followed by the main question, which includes the SMILES string and structure of the target molecule, generated with RDKit.

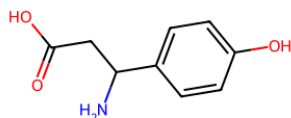


Image Prompt

You are an expert chemist, your task is to generate descriptive captions for molecules based on their chemical structure and properties.

General Outline

Given the Smiles string and molecular properties above, generate a descriptive caption for this molecule. The caption should describe the molecular structure, functional groups, potential applications, and any other relevant chemical properties. Be specific and technical in your description.

Task Instruction

Example 1:
Smiles: Nc1ccc(N)cc1
Description: The molecule is a phenylenediamine in which the amino functions are at positions 1 and 4 of the benzene nucleus. It has a role as a hapten, a dye, a reagent and an allergen.

Example 2:
Smiles: CCCCCOC(=O)c1ccccc1C(=O)O
Description: The molecule is a phthalic acid monoester obtained by formal condensation of one of the carboxy groups of phthalic acid with the hydroxy group of pentanol. It has a role as a xenobiotic metabolite, an anti-estrogen and a rat metabolite. It derives from a pentan-1-ol.

Examples

You are instructed to predict the target description caption of the molecule below. You are provided with the image of the target molecule below as a reference. Use the visual information from the image to support your analysis and reasoning, helping you generate a more accurate and comprehensive description caption of the molecule.

Question

Target Molecule (Smiles):
NC(CC(=O)O)c1ccc(O)cc1
Description:

The molecule is zwitterionic form of 3-amino-3-(4-hydroxyphenyl)propanoic acid arising from migration of a proton from the carboxy to the amino group; major species at pH 7.3. It has a role as a bacterial metabolite. It is a tautomer of a 3-amino-3-(4-hydroxyphenyl)propanoic acid.

Answer

Figure 20: **Example Molecular Description prompt:** The figure outlines a task for predicting the Molecular Description based on their SMILES string representation, using the ChEBI dataset. The general outline and specific instructions requires a captioning output.

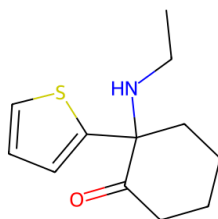


Image Prompt

You are an expert chemist, your task is to predict the property of molecule using your experienced chemical property prediction knowledge.

General Outline

You are an expert chemist tasked with predicting whether a molecule can penetrate the blood-brain barrier (BBB) based on its structure. Please follow this step-by-step reasoning process:

1. Analyze the molecular representation:
 - Identify key functional groups
 - Note molecular size and lipophilicity indicators
 - Look for charged groups or ionizable centers
 2. Consider important factors for BBB penetration:
 - Molecular weight (optimal range: 400-500 Da)
 - Lipophilicity (LogP between 1-4)
 - Number of H bond donors (<3) and acceptors (<7)
 - Polar surface area (optimal <70 Å...Å²)
 - Rotatable bonds (preferably <8)
 3. Examine structural features:
 - Check for presence of aromatic rings
 - Identify potential P-glycoprotein substrates
 - Look for CNS-unfavorable groups (acids, quaternary amines)
 4. Assess drug-like properties:
 - Evaluate adherence to Lipinski's Rule of Five
 - Check for presence of known BBB penetration enhancers
 - Consider potential metabolic stability
 5. Compare to known BBB penetrators and non-penetrators:
 - Analyze structural similarities with example molecules
 - Note any significant structural differences
 - Consider known structure-activity relationships
 6. Weigh the evidence:
 - List factors favoring BBB penetration
 - List factors opposing BBB penetration
 - Consider the overall balance of properties
 7. Make a prediction:
 - Based on your analysis, predict BBB penetration
 - State your final prediction as either "Yes" (penetrates) or "No" (does not penetrate)
- Please provide your reasoning for each step before giving your final prediction.

Task Instruction

Now, predict the BBB penetration for the following molecule:

Smiles: C1=C(SC=C1)C2(C(CCCC2)=O)NCC
 Penetration:

Question

Please follow the steps outlined above and provide your reasoning for each step before giving your final prediction of Yes or No.

Yes

Answer

Figure 21: **Example CoT prompt:** The figure outlines a task for predicting the Brain Penetration of molecules based on their SMILES string representation, using the BBBP dataset. The general outline and specific instructions requires a binary output (Yes/No).